Understanding and controlling the nucleation and growth of metal-organic frameworks

Brooke P. Carpenter, A. Rain Talosig, Ben Rose, Giuseppe Di Palma, and Joseph P. Patterson, Patterson, Patterson, Irvine, Irvine, CA 92697-2025, United States

Corresponding author email: patters Quei.edu

Abstract

Metal-organic frameworks offer a diverse landscape of building blocks to design high performance materials for implications in almost every major industry. With this diversity stems, complex crystallization mechanisms with various pathways and intermediates. Crystallization studies have been key to the advancement of countless biological and synthetic systems, with MOFs being no exception. This review provides an overview of the current theories and fundamental chemistry used to decipher MOF crystallization. We then discuss how intrinsic and extrinsic synthetic parameters can be used as tools to modulate the crystallization pathway to produce MOF crystals with finely tuned physical and chemical properties. Experimental and computational methods are provided to guide the probing of MOF crystal formation on the molecular and bulk scale. Lastly, we summarize the recent major advances in the field and our outlook on the exciting future of MOF crystallization.

1. Introduction

Metal-organic frameworks (MOFs) have become one of the largest and fastest growing research fields since the material was first introduced in the late 1990's.¹ Composed of metal nodes connected with organic ligands, MOFs have attracted popularity due to their incredibly high surface area, with some obtaining surface areas greater than the area of a football field per gram of material (~7800 m²/g).² These high surface areas make MOFs perfect for storage of large amounts of gaseous guest species such as hydrogen³ or carbon dioxide.⁴ MOFs also enjoy greater synthetic flexibility when compared to other porous materials like zeolites, which are currently used in many applications but have limited catalytic usage due to a narrow range of synthetic precursors.⁵ In contrast, MOF coordination networks can be synthesized from many different transition metals and linkers and can be easily tuned to obtain crystals with varying chemical functionality and porosity, allowing small molecules and biomolecules to be selectively adsorbed or encapsulated.^{6–8} Because of this synthetic diversity and ease of tunability, MOFs are now being studied for applications in almost every major industry, including catalysis,⁹ gas storage,¹⁰ sensors,¹¹ and drug delivery.^{12,13}

While high throughput screening methods can be credited for accelerating the synthesis of new MOFs (>90,000 recorded MOFs),14 currently only a limited number of MOFs are actually in industrial usage due to limited knowledge in how synthetic scaling and how high temperature and pressure processing techniques affect MOF formation and final structure. 15 The zeolite community—which has exploded in catalysis applications in the past two decades—has demonstrated that mechanistic studies on how a material forms enables its advancement, even with the limited catalytic applications this material has when compared to MOFs. 16-18 Additionally, the commercialization of most pharmaceutical drugs can be largely credited to mechanistic studies of drug formation as the studies were used to tailor drugs with specific surface chemistries and properties. 19,20 Most studies on the nucleation and growth of MOFs have been from the perspective of crystal growth, focusing on the rate of crystal formation, precursor phases, and crystal morphologies, rather than a molecular chemistry approach, focusing on bonding. ²¹ Extensive mechanistic studies have been performed only on a limited number of MOF systems, and they have found MOFs formations to often be complex, not fitting conventional crystallization models.^{22,23} Large-scale studies need to be performed to generalize these findings, which is challenging due to multiple intermediate phases occurring for each MOF synthetic condition. These phases need to be identified and characterized to better predict dominant MOF pathways. Additionally, how the reaction solution influences the formation and dynamics of the various intermediate phases has yet to be fully realized. Thus, a combination of ex-situ and in-situ studies are essential to gain a holistic understanding of the reaction dynamics and mechanisms of MOF synthesis on both the molecular and bulk scale. Such mechanistic studies will enable tighter control of MOF synthetic conditions and provide translatable findings for other materials. This review encompasses how we currently understand, control, and monitor MOF crystallization mechanisms, specifically focusing on zeolitic imidazolate frameworks (ZIFs), a class of MOFs which are structurally similar to zeolites and are widely studied. Additionally, we will provide our outlook on the future directions of the field.

2. Understanding MOF nucleation and growth

2.1. Nucleation and Growth Theories and Models

Crystallization studies have proven to be an important area of research in synthetic materials such as MOFs and across many natural systems occurring in biology and geology. Through these studies, scientists have extracted key thermodynamic and kinetic factors that unlock how atoms, ions, and molecules can pack to obtain final crystals with targeted properties. Three broad approaches are used, either alone or in combination, to model MOF nucleation and growth: classical nucleation theory, nonclassical nucleation models, and the SBU model.

2.1.1. Classical nucleation theory

Since the early 20th century, classical nucleation theory (CNT) has served as a theoretical framework for understanding the rates and mechanisms during crystallization. ^{24–26} The theory breaks crystallization down into two main categories: nucleation and crystal growth. Nucleation describes the assembly of monomers (atoms, ions, or molecules) into the smallest thermodynamically stable structure which possesses a crystalline lattice, known as a crystal nucleus. The key principle for nucleation is that there is a significant energy barrier to the formation of stable nuclei. This barrier is determined by two competing factors: Surface or interfacial energy and bulk energy. ²⁷ The interfacial energy is always a positive term as it is the origin of the nucleation barrier due to the fact that it requires energy to make an interface. The bulk energy is always a negative term as it denotes a release in energy or stabilization of the nuclei. The idea is to use enthalpy and entropic strategies such as manipulating bond strengths and degrees of freedom of MOF precursors to minimize the interfacial energy term. If the interfacial energy is too high, a nucleus cannot be formed and precursors remain in solution or bulk phase. If the interfacial energy is reduced, the nucleation barrier becomes manageable and crystal growth can proceed. Crystal growth occurs on the downhill slope of the energy barrier and involves the addition of monomers to the surface of the growing crystal lattice. The key principle for crystal growth is that monomers will tend to add to different crystal faces at different rates, which controls the morphology of the crystal as it grows. This growth often occurs through Ostwald Ripening, which refers to a phenomenon in which smaller particles of MOF precursors dissolve and add onto the surface of the growing crystalline phase. ²⁸

2.1.2. Nonclassical nucleation models

While CNT is essential to understanding how MOFs form, it has only been able to describe a few MOF systems.^{29–31} Most MOF crystallizations are categorized as non-classical, as they include intermediates and irregular final crystal structures and morphologies that cannot be explained with CNT. Additionally, MOF crystals often form metastable phases, which are a local energy minima in the MOF formation reaction (Figure 1).^{22,32} These metastable phases have broad definitions as they can be characterized as molecular clusters,³³ crystalline nanoparticles,³¹ liquids,²² kinetic polymorphs (which later evolve to a more thermodynamically stable, often nonporous polymorph),³⁴ and amorphous species.²³ The behavior of this metastable phase has significant consequences of the final MOF's characteristics, as it aids in establishing a degree of local supersaturation for the critical nucleus to form and start the nucleation process. Metastable phases have been observed to form when precursors concentrate and phase separate from the bulk solution to form solute-rich and solvent-poor areas. The solute-rich area then condenses into species such as amorphous particles and/or dense-liquid phases,23 which serve as the metastable phase (Figure 1). Once the metastable phase is formed, an energy barrier must be overcome for the metastable phase to transition into a critical nucleus for the final crystalline phase. While this transition is challenging to probe, the critical nucleus can form through the aggregation of the metastable phase, which is based on attractive forces of phases at close distances. If the metastable phase is of amorphous character, this transition is often called the amorphous-to-crystalline (ATC) pathway, which is a common mechanism observed in zeolites, 35 biomimetic polymers, 36 and magnetite. 37 Additionally, this transition into a critical nucleus can occur when disordered Metal-Ligand-Metal bonds rearrange into an ordered, crystalline structure. In this case, nucleation occurs within the rearrangement of Metal-Ligand-Metal bonds. Once a critical nucleus has been reached, MOFs have been observed to or through particle attachment, 23 where amorphous particles attach to the growing crystal in no particular orientated preference. Additionally, they can grow through oriented attachment (OA),31 where crystalline precursors attach to the critical nucleus through alignment of their lattices to the growing crystal.³⁸

2.1.3. The Secondary Building Unit (SBU) model

The nucleation and growth of MOFs can also be described by the secondary building unit (SBU) approach.^{39–41} SBUs are the molecular complexes from which the extended frameworks of MOFs are derived, and as such, they are the smallest possible assemblies of MOF precursors, consisting of single or multiple metal nodes coordinated to organic linkers.⁴² In these coordination complexes, the metal node acts as the vertex and the organic linkers act as the edges that join the vertices together, locking the metal node into a fixed geometry which lends itself to the rigid framework. SBUs can be classified by points of extension, defined as the number of possible metal connections between the organic linkers.⁴³ SBUs are also sometimes referred to as prenucleation clusters (PNCs) - which can refer to any species present in MOF synthesis reactions before nucleation – but here, PNCs which contain only metal nodes and organic linkers are referred to as SBUs.

In the SBU model of MOF nucleation and growth, SBUs form via coordination chemistry between nodes and linkers and aggregate via coordination linkages into a critical nucleus. This critical nucleus then grows into the final MOF crystal through the incorporation of more SBUs. This model is supported by a study of the MIL-n MOF family by Fe K-edge extended X-ray absorption

fine structure (EXAFS), which revealed that SBUs are present during both the nucleation and growth of MOFs, retaining their connectivity and structure throughout.⁴⁴ The formation of the SBUs themselves has been studied in systems including Mg-carboxylate MOFs,⁴⁵ ZIF-8,⁴⁶ MIL-101,⁴⁷ UiO-66⁴⁸, In-MIL-68⁴⁹, ZIF-67⁵⁰, MOF-2/MOF-5⁵¹, and SIFSIX-3-Zn⁵² using a variety of techniques from Electrospray Ionization - Mass Spectrometry (ESI-MS) and UV-visible spectroscopy to pair distribution function analysis and single molecule electron microscopy. These studies have shown that SBUs can assemble through a variety of mechanisms, such as ligand exchange and elimination at a single metal node, ⁵⁰ chain growth from a single metal node and linker, ⁴⁹ or organic linker coordination to inorganic metal clusters. ⁴⁸ These studies have also shown that not all MOFs follow the SBU model; specifically, the critical nucleus of ZIFs like ZIF-67 is not likely formed from SBU aggregation due to the tetrahedral geometry of the metal node in the final MOF and mixed geometry of SBUs found in solution during nucleation.⁵⁰

SBUs can arrange into a large library of geometries which have direct implications on the structural properties of a crystal.⁴¹ The stability, structure, and rigidity of SBUs can be tailored using factors further explored in section III, offering a promising area of MOF research. As the smallest possible assembly of MOF precursors, SBUs dictate the fundamental structure of the MOFs they make up. Thus, through the design of SBUs with appropriate geometries and sizes, final MOF properties such as network topology, stability and porosity can be controlled. This rational design of MOFs is a departure from previous high-throughput brute force methods which have been responsible for many MOF discoveries. ⁵³ As an example, Park et al used the principles of SBU design to produce MOFs with a new topology, *ssp*, by manipulating the structure of the organic linker to include a delocalized electron hole, showing that rational design of MOFs for specific uses is possible.⁵⁴ This concept of rational MOF design has already transformed the understanding of surface effects on MOF nucleation and growth, where the SBU approach has been used to model the interactions between MOF precursors and biomolecules to inform encapsulation, as has been done in BSA@ZIF-8 studies.⁵⁵

MOF growth from SBUs can be described by two mechanisms analogous to polymer growth: chain or step growth.³¹ In chain growth mechanisms, single SBUs add like monomers to the growing ends and facets of a crystal. In step growth mechanisms, SBU dimers, longer oligomers, and/or smaller crystals add to each other through oriented attachment.²⁴ The latter mechanism has been probed in the ZIF-67 system through molecular dynamics simulation, optical spectroscopy, and ESI-MS, giving insight into the molecular interactions that take place during SBU addition.⁵⁰ This study also found that complexes which can initiate nucleation are different from those which can initiate growth, both in how they form and in structure. ⁵⁰ This is not always the case; In the UiO-66 system, SBUs form a critical nucleus upon heating, and add to the growing nucleus, ordering themselves into the final MOF with time. ⁴⁸ Understanding how SBUs form, aggregate and incorporate into MOFs is crucial to describing the growth and especially nucleation of these materials, and we expect SBU formation to continue to play a key role in discovery of new MOFs and control of established ones.

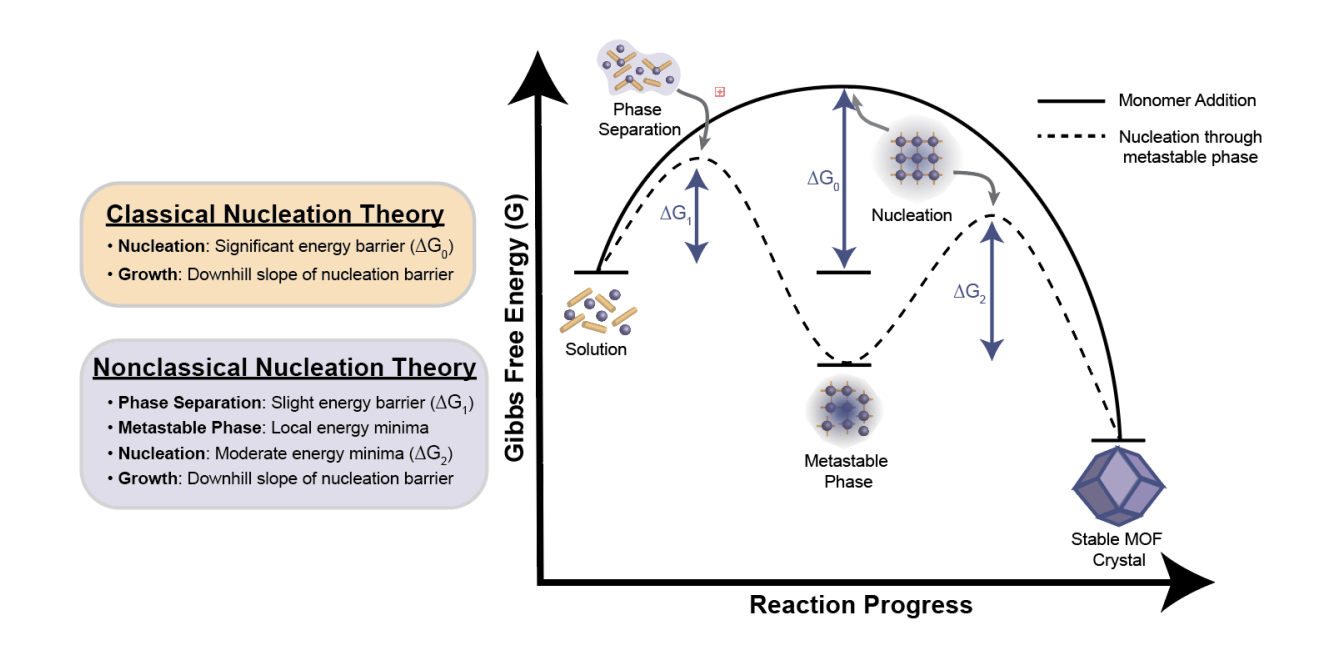


Figure 1: Free energy diagram comparing monomer addition (classical nucleation theory) and nucleation through metastable phase (nonclassical nucleation theory) mechanisms.

2.2. Kinetic Models of MOFs

While the previously mentioned models describe the mechanics of MOFs nucleation and crystal growth, it is also necessary to investigate their crystallization kinetics. X-ray Diffraction techniques (described in **Section IV**) are frequently used to exploit MOF crystallization kinetics. Data from this technique are coupled to fit two quantitative kinetic models: Avrami and Gualtieri. Originally, Avrami was a model used to describe crystallization by solid-state transformation, and it later evolved to describe solvothermal crystallization. The Avrami equation is expressed as:

$$\alpha = 1 - exp\left[-(kt)^n \right] \tag{1}$$

where α is the extent of crystallization, k is the crystal growth rate constant, t is the reaction time, and n is the Avrami exponent related to the dimensionality and the crystal growth. A significant limitation of this model is that it does not make a distinction between the nucleation and the growth step. The Avrami model assumes that crystallization occurs by adding individual molecules at a constant rate. For in contrast to the Avrami model, Gualtieri separates the rates of nucleation and crystal growth, as it was originally developed for zeolite synthesis analysis. The Gualtieri model can expressed by the equation:

$$\alpha = \frac{1}{1 + exp \left[- \left(\frac{t - a_N}{h_N} \right) \right]} \left\{ 1 - exp \left[- (k_g t)^{n_G} \right] \right\}$$
 (2)

The Gualtieri expression describes the extent of crystallization (α) as a function of time (t), growth rate constant (k_g), and crystal growth dimensionality (n). For example, if a crystal with tetrahedral geometry forms, the growth dimensionality (n) would equal 3 as this geometry is 3-dimensional. The fitting parameters a_N , which is the reciprocal of the nucleation rate (k_N), and b_N , which is variance of the probability of nucleation distribution, can then be used to calculate the nucleation and crystallization probability. A b_N value below 15 indicates heterogeneous nucleation; a value of 20 indicates homogeneous nucleations; and a value greater than 20 indicates autocatalytic nucleations. The nucleation probability is determined using the fitting parameters a_N and b_N using the following equation:

$$P_N = exp\left\{-\frac{(t-a)^2}{2h^2}\right\} \tag{3}$$

While the majority of the experimental data used to fit into these models are obtained from XRD techniques, a study by Filez et demonstrated that the Gualtieri model could be fit to curves in an in situ VIS spectra. Through the model, the nucleation distributions could be predicted. Additionally by fitting the model to curves from different synthetic ratios of the ligand:metal, trends relating to how change in ligand:metal affects nucleation and growth rates could be determined.⁵⁰ In summary, while the Avrami and Gualtieri models have been extensively applied to MOF crystallization, Avrami is often inadequate in characterizing MOF kinetics due to it being too general. Gualtieri, on the other hand, is more specific and can make distinctions between the nucleation and crystal growth rates.²¹ However, information relating to the nucleation energy barrier and to how synthetic parameters such as concentration and temperature affect the barriers cannot be obtained from either model.

Within the last few years, the microkinetic model has been introduced, which takes into account the SBU approach rather than the traditional classical and nonclassical nucleation and growth theories. While the Avrami and Gualtieri models focus on nucleation and crystallization rate and probability, and still provide useful information for MOF nucleation and growth, the microkinetic model extrapolates fundamental mechanisms occurring at the different steps in a crystal's formation. The model breaks the mechanisms down into 3 main steps: initiation of SBUs, chain and step growth, and termination. By breaking the mechanisms into 3 different steps, the activity energy barrier for initiation can be solved along with the rate constants for both the initiation and growth reactions.³¹ A key benefit of the microkinetic model is that it can further relate the nucleation rate to reaction conditions such as temperature and concentration of precursors using the following equation:

$$\dot{N}(\xi,T) = k_{0,n} \, \xi^{A_n} (1-\xi)^{B_n} exp(-\frac{\Delta G_n}{pT})$$
 (4)

In Eq. 4, \dot{N} represents the rate of nucleation in units of per second while ξ is the reaction extent. T represents the temperature in units of Kelvin, and $k_{0,n}$ is the pre-exponential factor of the nucleation rate constant k_n in units of per second. A_n and B_n are rate orders with A_n being with respect to the reaction extent and B_n with respect to the limiting reactant. $\Delta G_n(\text{J mol}^{-1})$ represents the activation energy required for nucleation, and R (J mol^{-1} K⁻¹) is the gas constant.

For example, the authors who created this equation demonstrated that by increasing the temperature of a system, the ratio of the chain to initiation rate can be used to predict the induction period and concentration of SBUs that can be used in the growth step. Additionally, the equation can be used to determine how increasing or decreasing the concentration of MOF precursors affects the initiation rate and concentration of SBUs that can be used in the growth step. The microkinetic model can further extract information regarding rate of MOF growth and the reaction order with the following equation:

$$G(\xi,T) = k_{0,n} \, \xi^{A_g} (1-\xi)^{B_g} exp(-\frac{\Delta G_g}{PT})$$
 (5)

 $G\left(\xi,T\right) = k_{0,n}\,\xi^{A_g}(1-\xi)^{B_g}exp\left(-\frac{\Delta G_g}{RT}\right) \tag{5}$ In Eq. 5, G represents the rate of growth in units of meters per second. $k_{0,g}$ is the pre-exponential factor of the growth rate constant k_g in units of per second. A_g and B_g are rate orders with A_g being with respect to the reaction extent and B_g with respect to the limiting reactant. ΔG_a (J mol⁻¹) represents the activation barrier required for growth.

By extracting the growth rates from this equation, crystal size and dispersity can be predicted. Furthermore, the microkinetic model can be used to describe mechanisms leading to crystal termination. For example, the authors who created this equation demonstrated that the termination step was caused by decreasing the reactivity of the MOF surface. While the microkinetic model definitely provides significant mechanistic insights, Flory's approximation is used to predict the bond strength for the growth step of the model, which does not take into account size dependence of the clusters or aggregates as the size of aggregates can influence overall binding strengths. Additionally, as MOFs can develop crystal defects, future work is needed to develop a kinetic model that can integrate defect mechanisms.

2.3. Polymorphism in MOFs

MOFs can exhibit polymorphism, where MOF crystals can consist of identical chemical composition but differ in their network topology.⁶¹ As a result, multiple crystalline phases of MOFs can be produced with different symmetries and densities. By tuning the activation energy of the MOF through changing synthesis conditions, higher energy products can be kinetically trapped at low activation energy barriers or the reaction can proceed to the lower energy thermodynamic products at high activation energy barriers; thus polymorphs can be found at different energy minimas of a free energy landscape diagram.⁶² Since polymorphs can display different crystal structures while retaining identical molecular composition, the structure-function relationship based on structural parameters can be investigated. ^{63,64} Polymorph transition can be induced post-synthesis through physical steps like additional heating,⁶⁵ pressure, or template mediation.⁶⁶ Typically, post-synthetic phase transitions result in the formation of more dense, thermodynamic crystalline phases through reconstruction or displacement of internal structures. 63 For example, washing of ZIF-8 MOFs synthesized in water with alcohol solvents can initiate phase change from ZIF-C and ZIF-L to ZIF-8 (sod), ^{67,68} Additionally, intrinsic and extrinsic synthetic conditions can control the competition among polymorph phases during the MOF formation.⁶⁹ For example, the use of template vapors in chemical vapor deposition enables control over the formation of a porous or nonporous ZIF polymorph.66

While polymorphism is often not screened in MOF studies, mechanistic studies of zeolites, which have ~250 different polymorphs,⁷⁰ have aided in polymorph control of MOFs, as the metal-ligand coordination in ZIFs are similar to the building units of inorganic zeolites. Whereas zeolites are composed of SiO₄ and AlO₄ units, ZIFs have tetrahedral metal centers, commonly divalent metals such as Zn²⁺ or Co²⁺, that are bridged with imidazolate ligands. Consequently, ZIFs share many of the same network topologies and rich polymorphisms as zeolites.⁷¹ In all zeolite polymorphs' formation reactions, primary amorphous phases form, followed by secondary amorphous phases. Recent computational studies have determined the rate in which this secondary amorphous phase grows into a crystalline phase determines the final polymorph selection.⁷² Polymorphs with distinct physical properties can be produced by altering the packing density of the building units as well as the orientation of the imidazolate units. For example, ZIF-8 sodalite (sod), which is the most widely studied kinetic polymorph of ZIF-8, is the least densely packed, resulting in large pores (~11.4 Å) that are ideal for encapsulating guest molecules.⁷³ In contrast, ZIF-8 diamondoid (dia), which is the most thermodynamically stable polymorph, is the most densely packed and not ideal for encapsulating guest molecules. Polymorphs of ZIFs can be revealed through in-situ monitoring techniques such as in situ PXRD, which allowed for the observation of a new metastable ZIF-8 polymorph generated through mechanochemical milling, kat.34 Additionally, cryo-TEM studies have shown amorphous particles emerge for the formation of ZIF-8 (sod) and dia polymorphs.²³ While these TEM studies have also shown that the amorphous particles undergo a redissolution-crystallization mechanism for sod, a separate mechanism is suggested for *dia* formation that requires further exploration.

2.4. Summary:

The field of nucleation and growth is well established, and while there has been significant progress made in understanding the nucleation and growth of MOFs, there is still much work to be done. While all MOFs are assembled via

coordination chemistry, the mechanism by which this occurs can be different for each MOF and can change with different synthesis conditions. While some MOFs' nucleation and growth can be described using classical nucleation theory, others require different theoretical frameworks like SBU addition and/or OA, or a combination of several. In a similar fashion, the mathematical models used to properly describe both MOF nucleation and growth are not universal; different MOF systems can be described by different equations. Understanding the different MOF systems' different mechanisms is essential in the development of a unifying theory describing the nucleation and growth of these exciting materials. Specifically, more work is needed to understand the molecular chemistry for all MOF classes, and more work should be done to expand nucleation and growth for different classes of MOFs. In the case of ZIFs, while much is known about the nucleation and growth of these composites, there are still many unanswered questions. The formation mechanisms of many ZIF polymorphs—such as the thermodynamically formed dia and carbonate-incorporating ZIF-C—are not understood. We predict that further examination of the nucleation and growth of ZIFs specifically, perhaps guided by previous work studying zeolites, will help in the understanding of similar other MOF systems' nucleation and growth, like MAFs, or Metal Azolate Frameworks.

3. Controlling MOF nucleation and growth

The MOF nucleation and growth reaction can be controlled through manipulating phase changes during synthesis. Phase change of a system occurs when the total free energy of the proceeding phase is less than the total free energies of the prior phase. Intrinsic and extrinsic parameters can dictate whether a phase transformation is energetically favorable through increasing or decreasing the free energy barrier to nucleate a particular phase. Intrinsic factors refer to the internal properties within a MOF system, such as the chemical composition and concentration of the precursors, along with temperature and reaction medium. Extrinsic factors include the presence of foreign surfaces, small molecule modulators, and confinement, which can directly affect the surface energy barrier to nucleation. Extrinsic factors frequently control the rates and mechanisms of MOF by favoring a type of nucleation called heterogeneous nucleation, which occurs outside of the bulk solution such as on a foreign surface. Heterogeneous nucleation enables nucleation to occur at lower supersaturation conditions, resulting in increased rates of nucleation compared to nucleation occurring in the bulk solution (homogeneous nucleation).⁷⁴ Much has been written about the effects of different synthetic conditions on final MOF size and quality. In this section, we use these final properties to extrapolate information about MOF nucleation and growth mechanisms. Some properties mentioned in this review which can be tied to nucleation and growth include metal-ligand bond strength (which relates to both nucleation probability and to growth),75 crystal size (which can relate to the relative nucleation and crystal growth rates), ⁷⁶ crystalline defects (which indicate errors in SBU formation and/or arrested growth), and crystal polymorph (which can be used to tell whether a reaction is thermodynamically or kinetically controlled). ²³ Both intrinsic and extrinsic factors will be discussed in more detail in this section.

3.1. Chemical composition and medium

Both MOF composition and solvent play significant roles in both the nucleation and growth of MOFs. The strength of the metal-ligand bond, which is essential to the assembly of stable SBUs, can be modulated based on electron sharing between the ligand and metal. When choosing a ligand, factors to consider are the electron- withdrawing and electron-donating effects. For example, ZIF-8 has a stronger Zn-N coordination than ZIF-108, as the ligand in ZIF-108, 2-nitroimidazole, has a greater electron-withdrawing effect on the imidazole ring, and thus greater Zn-N bond length than the ligand in ZIF-8, 2methylimidazole.⁷⁷ The different strength of the Zn-N bond in different Zn-based imidazolate MOFs provides different applications for the materials; while stronger Zn-N bonds are desired for storage applications, weaker bonds can facilitate reversible phase transformation, which broadens the material's applicability. 78 Indeed, ZIF-108 undergoes metal substitution much easier than ZIF-8 does, the latter of which requires a base to prevent phase transformation during this process 77,79. This suggests that the rate of growth should be higher for ZIF-8, as hydrolysis-resistant metal-ligand bonds lead to higher crystal growth rates. When choosing a metal, the Irving-Williams series can be used to determine the strength of divalent metals complexes in water.^{80,81} This series is often explained based on the ionic radius of a divalent metal and the crystal field stabilization energy of a complex. For example, Cu2+ is expected to form a more stable metal complex than Zn 2+ based on the smaller ionic radius of Cu²⁺. Of course, to measure MOF nucleation and growth, a given metal and linker must be able to form a MOF. While this may seem obvious, many metal-ligand combinations will not produce MOFs, meaning selection of a linker for a corresponding metal node must be done with care. When designing the metal-ligand combination for a MOF, Pearsons's hard-soft acids and bases (HSAB) theory must be utilized, as the binding strength and stability of the metal and ligand bond drives the self-assembly process and dictates the final performance of a MOF.82 Hard metals such as Zr4+ form strong metal-ligand complexes with strong bases such as carboxylate ligands, and soft metals such as Zn2+ form strong metal-ligand complexes with weak bases such as

azolate ligands.⁸³ Borderline metals such as Cu^{2+} can interact with both strong and weak bases, examples being benzene-1,3,5-tricarboxylate, a strong base, and 2,2'-dipyridyl, a weak base, in the case of the HKUST-1 and $[Cu(4,4'-DP)_{0.5}Cl]_n$ frameworks respectively.^{84–86} Different linkers and metals will display different nucleation and growth kinetics, the understanding of which varies between MOF systems.

Metal-ligand bond strength cannot be discussed in a vacuum; the reaction solution, and specifically the solvent, is critical for dictating the metal and ligand coordination environments. Furthermore, MOF's can only self-assemble into crystalline units if the metal-ligand bond formation is more energetically favorable than the solvent-ligand exchange rate. Solvent can play various roles in the self-assembly process. It can govern the rate and pathway of crystal formation, be incorporated into the MOF by coordinating with the metal ions, or both. In the case of water-stable ZIFs, the ΔG of hydrolysis must be a positive value, meaning that metal-ligand binding is more energetically favorable than the metal or ligand binding with water. By modulating the hydrophobicity of the ligand, the rate of ligand/solvent binding can further be tuned, as hydrophobic ligands have a lower rate of binding with water molecules.

The solubility of the ligand in the reaction medium plays an important role in the crystallization rate as a more soluble ligand facilitates increased nucleation and growth rate. For example, a study demonstrated this concept by using a ligand more soluble in DMF than in water and showed how the MOF crystallized much faster in DMF than water due to the ligand's high solubility in DMF.⁸⁸ The solubility of the ligand also can impact the network dimension of a MOF as it influences the binding affinity of the solvent molecules to the metal centers. For example, a study showed that through increasing ligand solubility, the solvent-metal binding consequently decreased, which resulted in an increase of the crystal dimensionality (i.e. 1D, 2D, 3D).⁸⁹ The rate and extent of deprotonation of the ligand further affects the self-assembly and final MOF structure and size. A study by Kim et al. observed larger particles formed in more polar solvents as more polar solvents have higher proton acceptance power.⁹⁰ As a result, the interfacial energy of the system decreases as the concentration of available ligands for metal coordination increases. With a higher concentration of available ligands, larger MOFs with high crystallinity can form. This is not only seen in systems with changing solvent polarity; in MOFs, lower metal-ligand binding (growth) rate equals larger particle size (Figure 2).

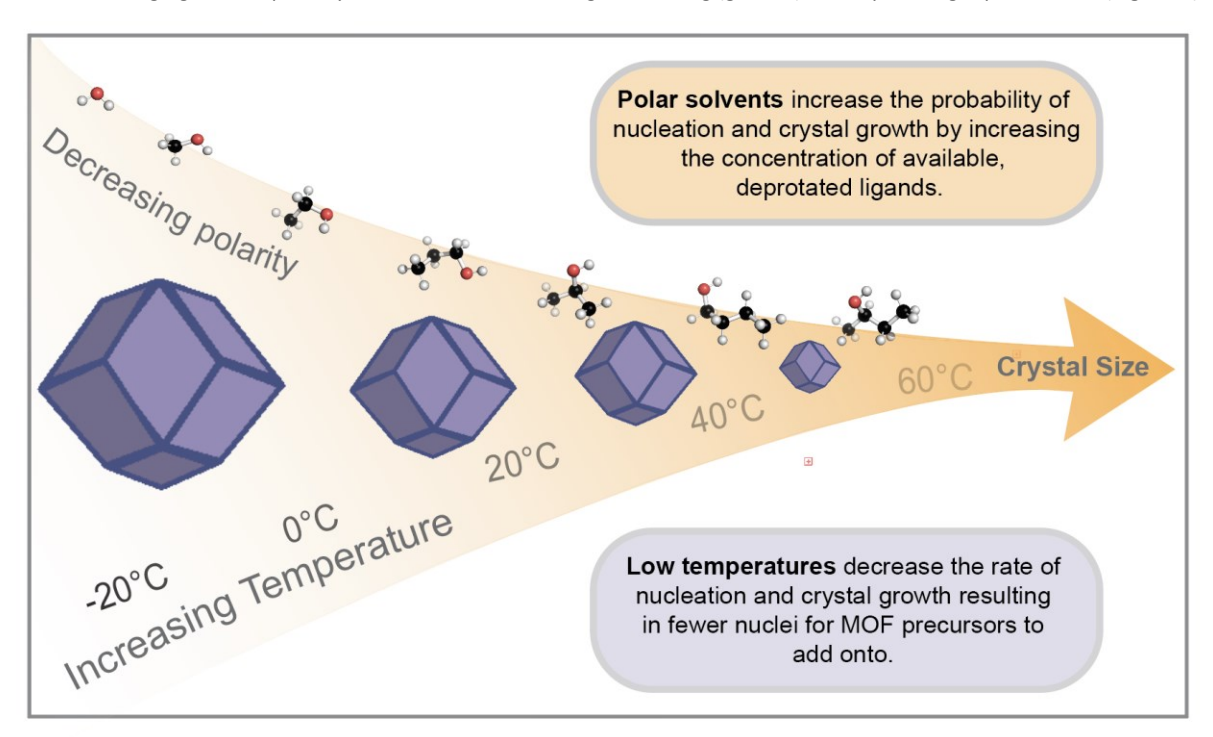


Figure 2: Particle size dependence on solvent polarity and reaction temperature

Functionalizing organic ligands allows for electronic and steric effects during self-assembly and in the final MOF product to be finely tuned. For example, by combining two complementary imidazole ligands, a study showed the organization and conformation of ligands in the initial building units could be tuned based on ligand size, as this influences ligand-ligand

interactions and, consequently, sterics.⁹¹ Ligands can further be functionalized in a way that does not alter MOF self-assembly, yet plays a greater role in the final properties of a MOF.⁹² As shown in early ZIF studies, increasing the length of the ligand directly increases the pore size without affecting nucleation and growth.⁵ Furthermore, a study done by Kim et al suggested that ligand rigidity directly affects final MOF stability and selectivity. In this study, researchers examined six ligands with varying rigidity, and found that the MOF synthesized with the most rigid ligand exhibited the best stability in water.⁹³

In addition to solvent polarity, the purity and ionic strength of a solvent affects the arrangement and size of the initial assembled clusters. For example, a pure aqueous solvent has been shown to facilitate fast nucleation and produce larger clusters compared to an aqueous solution with ions.³³ Additionally, free ions, such as Na⁺ and F⁻, in solution can dictate the extent of defects in a crystal structure.⁹⁴ This occurs as a result of the ions interacting with the MOF building units during growth, preventing ligands from rotating and consequently forming defects. Defect formation is most prominent at lower ion concentrations. As ion concentration increases, the probability of crystalline unit formation is decreased, due to an increased stability between the metal and counterion. Ions also can stabilize complexes during growth, raising the energy barrier to add more monomers or SBUs, which leads to defects and trapping of kinetic products. Ions can also add themselves into the crystal lattice of a MOF, as is the case with ZIF-C—where carbonate ions incorporate themselves into the ZIF-8 lattice during formation—changing the nucleation and growth mechanism in a way that is still not understood.

The concentration of precursors and ratio of ligand to metal is further key in MOF self-assembly mechanisms. Excess ligand drives nucleation in some ZIF systems through the deprotonation of building units, reducing the rate of hydrolysis. Increasing the extent of excess ligands speeds up the reaction rate, producing smaller kinetic products with low dispersity. Ogata et al. found that at high ligand-to-metal ratios, ZIF-8 is formed by adding amorphous nanoparticles. These precursors then follow a dissolution-recrystallization mechanism to form ZIF-8 (sod) crystals. Without excess ligands, protonated ligands remain in solution, causing the crystallization rate to decrease and the formation of thermodynamic phases such as dia. ^{23,95,96} In the same study by Ogata et al, it was found that ZIF-8 nanoparticles initially formed at low ligand-to-metal ratios, but that the nanoparticles appeared to be relatively stable, as no particle aggregation could be observed for the first 24 hours, after which ZIF-8 (dia) crystals formed. This further supports the idea that the crystallization rate decreases at lower ligand to metal ratios, and that ZIF-8 (dia) is the thermodynamic product of the ZIF-8 reaction.

3.2. Temperature

Temperature is another key intrinsic factor for controlling MOF nucleation and growth. The temperature of the MOF synthesis reaction dictates the ligand solubility and conformation as well as its extent of coordination to the metal node. Systems synthesized under high temperatures increase the chemical potential, $\Delta\mu$, within a system and have greater solubility of reactants and rates of metal-ligand bond formation as given by:

$$\Delta\mu = k_B T \sigma \tag{5}$$

$$\sigma = ln(AP/K_{sp}) \tag{6}$$

where k_B is the Boltzmann constant, T is temperature, σ is supersaturation, K_{Sp} is the MOF reaction's equilibrium constant, and AP is the activity product of the reactant.²⁷ It is important to note that there are other ways of defining both $\Delta\mu$ and σ , with some definitions of σ being given as approximations. ^{27,97,98}. Additionally, the temperature can dictate the probability of overcoming an energy barrier and stability of the final crystal. By increasing temperatures, the thermal energy within the system increases, resulting in a greater driving force for crystallization, specifically of the thermodynamic product, to occur. On the other hand, at lower temperatures, the thermal energy within a system is low, allowing for intermediates and kinetic products to be formed. A study compared ZIF-8 synthesized in methanol at 130°C and 25°C, and found the higher synthesis temperature facilitated a greater percent yield of MOFs, which indicates a greater rate of ligand/metal coordination.96 Target synthesis of MOF crystals with desired size, porosity, and morphology can be accomplished in part by obtaining a holistic understanding of how temperature influences MOF growth. The number of nucleating species and nucleation rate is greater at higher temperatures facilitating the formation of more nuclei and, consequently, crystals with smaller diameters. This theory is supported by a study that found that increasing the synthesis temperature from -15°C to 60°C caused the average diameter of ZIF-8 crystals to decrease from 78 nm to 26 nm.⁹⁹ In addition to controlling the nucleation and growth and crystal size, reaction temperatures can dictate the dimensionality of the final MOF crystal by controlling the rate of metal binding to ligand and solvent molecules. By increasing the temperature, crystals with greater dimensionality can be obtained as coordination to solvent molecules decrease, often resulting in the coordination number of the metal center to increase. 100

3.3. Surfaces

Surface substrates have shown great potential for nanoscale control of crystal formation, 101 aiding in the discovery of new types of materials for CO2 separation, 102 water splitting, 103 and field-effect transistors. 104 Surfaces control the self-assembly pathway of crystal formation by modifying the interfacial free energy barrier and offering a site for crystals to nucleate (Figure 4). 105 The effects of surfaces themselves on crystal growth are usually not as pronounced, although confinement by surfaces can noticeably affect growth of MOFs; this is discussed in a separate section. The extent of which a surface can modify crystal nucleation is largely dependent on two factors: 1.) atomic structure of the surface and 2.) the strength of the bonds formed by the MOF precursors and the surface. By matching the atomic structure of a surface to a desired lattice place of a crystal, surfaces can be used to control the orientation of the crystal lattice by minimizing the lattice strain in a desired orientation. Planar substrates include flat, smooth surfaces such as alumina¹⁰⁶ and silica^{107,108} and provide a uniform surface for MOFs to grow. These substrates often include self-assembled monolayers (SAMs), 109,110 that can be functionalized with different terminating groups to dictate the orientation of the MOF crystal. In a study by Shekhah et al, the authors describe studying the formation of metal-organic frameworks (MOFs) in a sequential fashion on a functionalized SAMs. 111 The surface of the SAMs was functionalized with mercaptohexadecanoic acid (MHDA) as the carboxylic acid groups matched with the (100) plane in the crystal lattice. As a result, the orientation and growth of the crystal could be controlled, resulting in homogeneous crystalline films. Furthermore SAMs can be functionalized with multiple different terminating groups which promotes nucleation of different lattice orientations. Such control of the nucleation enables the engineering of novel MOF structures with finely tuned lattice patterns. 112

Another aspect to consider when choosing a surface is the chemical composition of the surface interface. The interfacial chemistry can be used to modulate the binding strength of the MOF precursors to the surface, and consequently, the probability of nucleation. By the MOF precursors forming stronger bonds with the surface rather than with the solvent molecules, the interfacial energy barrier required for nucleation decreases.²⁷ The available surface area for strong-bonds to form can also impact the probability of nucleation. Non-planar substrates, which are surfaces that are more complex and have three-dimensional structures, provide a larger surface area for the MOFs to grow on, leading to faster formation and higher yields. 113-115 Examples of non-planar substrates include foams, 116 fibers, 117 nanowires, 118 proteins, 7,115,119,120 and porous metals. 121,122 A study by Ogata et al. used bovine serum albumin as a non-planar substrate to lower the interfacial energy barrier and tune the crystal morphology and structure.²³ In the study, cryo-TEM observed that a protein was capable of concentrating MOF precursors, forming amorphous protein/Zn/HmIm particles and, subsequently, ZIF-8(sod) crystals through a dissolution recrystallization mechanism. Otherwise, in the absence of protein, ZIF-8(dia), the nonporous and thermodynamically stable ZIF-8 polymorph, formed (Figure 3). The ability for the protein to drive crystal formation of ZIF-8 (sod)was strictly dependent on its negatively charged surface as other studies have shown that biomolecules with high isoelectric points (>7) cannot promote crystal formation. 115 With this insight, molecular modifications of proteins have shown to be promising methods for tailoring the surface chemistry to promote nucleation and growth of a particular MOF phase and morphology. 123 Furthermore, proteins are believed to add to the growing crystal through particle addition. Through addition, the proteins create defects in the crystal as they are too complex to match the lattice planes of the MOF.^{23,120} By controlling the size and concentration of protein particles, such defects can be tailored.

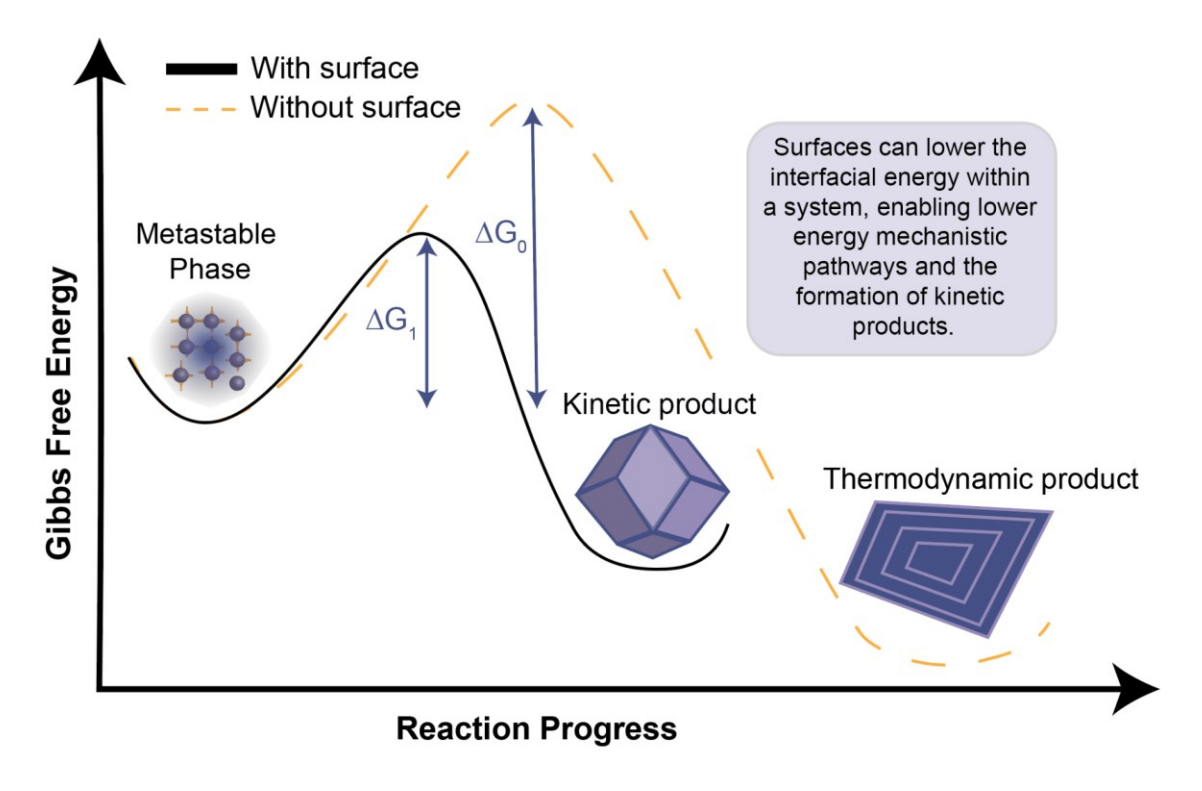


Figure 3: Comparison of free energy barrier in homogeneous (without surface) and heterogeneous crystallization (with surface). 124

Along with biomolecules, polymers can also serve as templates to regulate the crystalline phase, shape, size, and porosity of MOFs.¹²⁵ Ionic polymers offer many coordination sites for MOF nucleation, while instead, non-ionic polymers may self-assemble to influence the final MOF structure and porosity through electrostatic interactions. For example, through a coordination-modulation mechanism, a non-ionic block copolymer was able to trap a kinetic crystalline phase through stabilization of prenucleation aggregates. ¹²⁶ In summary, each type of surface has its own benefits for tailoring the nucleation and growth of MOF formation. For example, if a planar substrate is being used, a fabrication method may be developed that takes advantage of the flat and smooth surface of the substrate to help control the growth and formation of the MOFs in a precise and uniform manner. On the other hand, if a non-planar substrate is being used, a fabrication method may be developed that can adequately grow the MOFs on the more complex surface of the substrate, potentially leading to faster formation, higher yields, and trapping of kinetic products.

3.4. Small Molecules

The idea of using small organic molecules as structure-directing agents (SDA) to design porous frameworks has been well-established in the zeolite community. Additionally, SDAs are widely credited for the structural diversity of zeolites as they can embed into zeolite structures and influence the pores based on the chemical structure and size of the additive. Small molecules have been similarly used as modulators during the self-assembly of metal-organic frameworks (MOFs). These molecules, which can be organic or inorganic, can be added during the synthesis of the MOFs to stabilize kinetic products and control the resulting crystals' size, structure, and shape.

Acids and bases are common small molecule modulators for polymorph selection and crystal size, as they can either increase or decrease the rate of crystallization. For example, MAF-7, which uses triazolate linkers, only forms rhombic dodecahedron morphologies upon addition of ammonia. Otherwise, the interfacial energy required for crystallization is too high, and only amorphous products are formed.¹²⁹ The addition of a strong base greatly increases the supersaturation of the

deprotonated ligand (which is required for MOF formation) and decreases the interfacial energy required for nucleation. In contrast, Brønsted acids such as HCl or monocarboxylic acids can be used to increase the interfacial energy of a system as it increases the concentration of protonated ligands, resulting in a decrease in the rate of crystallization. Thus, fewer nuclei are formed promoting the growth of large, highly crystalline MOFs. For example, a study used benzoic acid to modulate the rate of crystallization of UiO-68-NH $_2$ and obtained crystals as large as 100 μ m. 131

Capping agents are types of small molecules that can selectively bind to a facet of a crystal. This type of modulator is able to affect both thermodynamic and kinetic factors of MOF growth. From a thermodynamics perspective, the structural morphology of a system can be estimated by the Wulff construction principle, where the crystal shape with the lowest surface energy will be formed.^{132,133} By adding onto a preferred facet of a crystal, capping agents can minimize the surface energy of that facet and alter the most stable structural topology. From a kinetics perspective, the morphology of a system is dependent on the rate of diffusion of monomers that are deposited onto a growing crystal.¹³⁴ Capping agents can act as a physical barrier for a particular facet, resulting in a decrease in the rate of monomers diffusing and depositing onto the facet decreases. Such mechanisms can facilitate the formation of higher energy, kinetic products. Examples of modulators used to tune the crystal size and morphology of ZIF-8 include organic amines¹³⁵ and surfactants.^{136,137} A study used by Pan et al used the surfactant cetyltrimethylammonium bromide (CTAB) to trap kinetic morphologies of ZIF-8.¹³⁸ In the study, CTAB preferentially adsorbed onto the {100} face causing a reduction of crystal growth in that direction. By increasing the concentration of CTAB, the capping effect was amplified, causing smaller particles with truncated cube morphologies to form rather than the typical rhombic dodecahedron morphology (Figure 4).

While small molecules can serve as capping agents, they can also serve as competing agents which promote the formation of larger crystals and the most thermodynamically stable morphology (i.e. the Wulff polygon). A study by Cravillon et demonstrated that small molecules, specifically monodentate ligands, can serve as competing agents that compete with the bidentate ligands to bind to the metal ions. In the study, target diameters of ZIF-8 nanoparticles could be achieved with addition of monodentate ligands (1-methylimidazole, sodium formate, or n-butylamine). Through addition of 1-methylimidazole or sodium formate, larger crystals (1 μ m) with narrow size distribution were formed, as the competitive binding decreases the rate of nucleation and growth. Furthermore, the particle size can be dictated by tuning the similarity of the ligand and modulator pKa as it is key to dictating the rate of binding to the metal node. Additionally, the presence of the monodentate ligands resulted in preference of the thermodynamic morphology (rhombic dodecahedra) over the kinetic morphology (cubes). In summary, by understanding how modulators can be used to control the activation energy barriers for nucleation and the growth rates, we can use them as tools to design MOFs with targeted shapes and sizes.

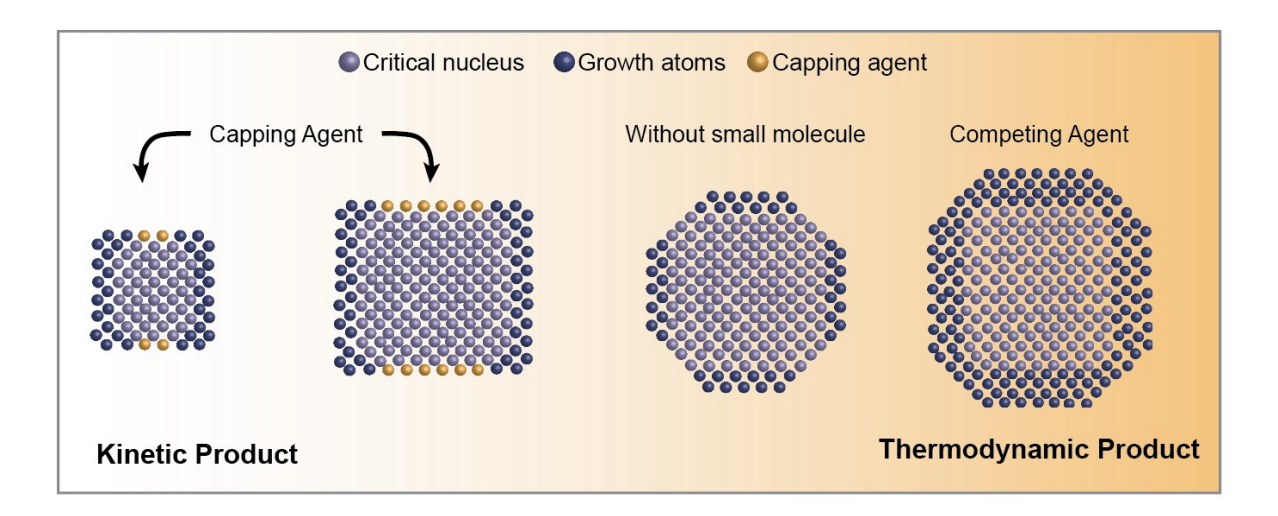


Figure 4: Schematic diagram of various kinetic and thermodynamic products associated with small molecules either serving as capping or competing agents during the crystal formation. With a small molecule acting as a capping agent, it is adsorbed onto a facet of a crystal resulting in square-shaped crystals. Depending on the binding strength of the capping agent, crystals of varying

sizes can be produced. Without a small molecule, hexagon-shaped crystals form. With a competing agent, MOF precursors are competing with a small molecule to bind to the growing crystal resulting in larger hexagon-shaped crystals.

3.5. Confinement and synthesis volume

Nanoscopic confinement has been widely used to design high-performance materials with hierarchical structure in the biomineralization community. Nanoscopic confinement influences occur in restricted volumes such as membranes and pores which can limit crystal growth in the x, y, or z dimensions. The confinement's character can significantly influence the nucleation rate and stability of intermediate phases. By increasing the degree of confinement on a system-lowering the volume where synthesis and crystallization can take place–studies have observed a decrease in the nucleation rate of crystallization. This decrease is due to a decrease in any impurities that could act as nucleators and volume is proportional to nucleation probability.¹³⁹

Nanoscopic confinement has been shown to stabilize metastable products and phases for non-MOF systems. For example, a study found that by increasing the degree of confinement during the crystallization of amorphous calcium carbonate, the amorphous phase was stabilized. This is due to the energy barrier for the thermodynamic product increasing. In addition to the degree of confinement affecting growth, the surface area of the synthesis vessel can have a further effect. For example, when a system is assembling in a porous confinement, a greater fraction of the nucleus will be in contact with the substrate and thus have a greater nucleation rate than in a system that occurs within flat confinement. On finement methods using various interfaces, such as colloforms and droplets, have synthesized MOF nanoparticles with high uniformity and low size distribution. The key to obtaining such products lies in having fast nucleation but slow growth. Synthesizing a MOF in a confined environment allows this to occur as it decreases the probability for nuclei to aggregate.

Confinement interfaces have shown the potential to serve as templates for controlling the growth direction of crystals by restricting growth in designated orientations. Many studies have succeeded with this method by using emulsion interfaces to confine MOF growth within a specific geometric mold. By varying the length of the surfactant in a reverse micelle system, ZIF-8 crystals with targeted sizes could be achieved. One specific study used an aqueous-organic liquid interface to mold HKUST-1, ZIF-8, and LnBT crystals into a wide range of crystal geometries such as hearts, circles, and rectangles. The ability to obtain each crystal geometry was based on localizing the nucleation and growth within molds of specific geometries. This mold was stationed at an opening in the interface surface where its shape could be altered by varying buoyancy and capillarity forces. In addition to emulsion interfaces being used to control crystal shapes, hard confinement surfaces can template MOFs with hierarchical structures and porosity. Synthesizing such hierarchical materials can be advantageous for catalytic applications as demonstrated with PCN-224 which was synthesized within the confinement of macroporous melamine foam to create geometry that promoted greater catalytic activity. 144

While studies have used nanoscopic confinement methods to synthesize MOFs with desired physical properties, future research is still needed to use confinement as a method to discover and trap metastable MOF products. Additionally, on the other side of the spectrum, nucleation and growth mechanisms that occur during macroscopic scaling of a MOF synthesis are currently unexplored. Such mechanistic studies are crucial for designing large-scale MOF synthesis using green approaches, as many current synthetic approaches in industry use toxic solvents and MOF precursors along with pressure-sealed reaction vessels, all of which pose high financial costs. ^{145,146} Recently, advances towards this challenge include a study by Deacon et al which investigated kilogram-scale production of ZIF-8 while using water as the solvent. The authors note that the crystals observed in the scale-up synthesis have distinctly different sizes than those reported in literature from small-scale synthesis. ⁶⁷ Such findings emphasize the impact that scaling has on final MOF crystals and the need for mechanistic studies.

3.6. Summary

Intrinsic and extrinsic factors are commonly used to control MOF formation by manipulating the MOF nucleation energy and growth rate. Intrinsic factors include chemical composition, medium and reaction temperature, and extrinsic factors include surfaces, modulators and confinement. Currently, there is a better understanding of intrinsic factors vs. extrinsic factors. Heterogeneous nucleation is a powerful way to control nucleation and growth, especially for applications in uses of MOFs like drug delivery or enzyme immobilization. Extrinsic factors are also extremely useful for finely controlling things like crystal size distribution, which is vital for applications like catalysis. We predict that the future studies of extrinsic factors on MOF nucleation and growth will become more important as the aforementioned applications of MOFs become more widespread.

4. Monitoring MOF nucleation and growth

The complexity of MOF nucleation and growth requires strategic experimental and instrumental methods to obtain a thorough understanding of the mechanisms and kinetics driving each intermediate and final phase. While no single instrumentation method can capture the broad spectrum of the crystallization process from initial building units to final bulk crystal, each instrument has its own strength as some instrumental techniques enable characterization of a specific, localized region and provide qualitative insight into individual crystal size and morphology, while other techniques may provide ensemble information and quantitative insight into the crystallization kinetics. Thus, multiple complementary instrumentation methods are required to obtain a holistic overview of the crystallization by providing descriptions of each phase and phase transition. Each instrument will be discussed in more detail in this section, and examples of how each technique can be used to monitor MOF nucleation and growth will be provided.

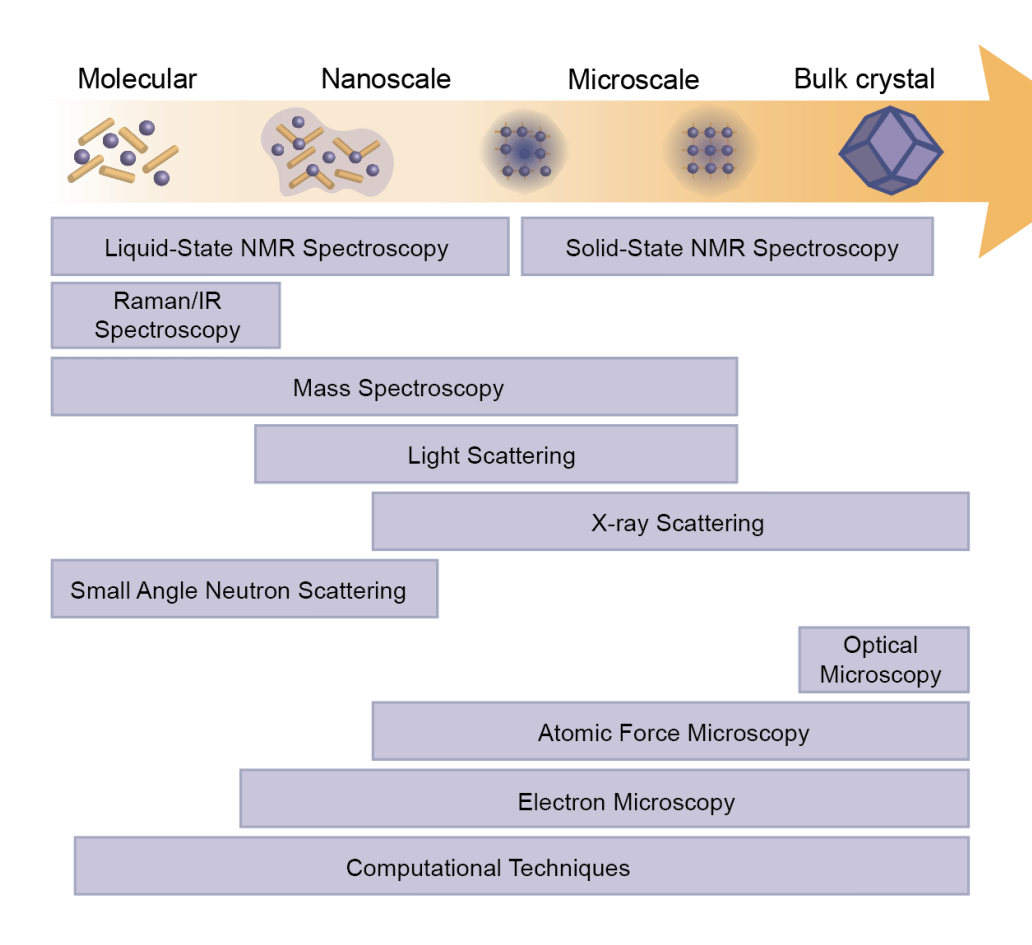


Figure 5: Summary of experiential and computational techniques to study nucleation and growth of MOFs and the phase regime that they are useful for probing

4.1. Mass Spectrometry and Spectroscopy Techniques

Mass spectrometry and spectroscopy techniques are the most widely used techniques among organic and organometallic chemists to provide characterization on chemical structure and interactions of small molecules. Spectroscopy operates through radiating a sample with photons and measuring the absorption of the radiation, which can then be used to determine properties of nuclei, bonds, or atomic orbitals, depending on the energy of the photon. Mass spectrometry measures the interactions between the sample and radiation, allowing the mass of a sample to be determined through its mass-to-charge ratio. Such measurements enable the study of the initial coordination among prenucleation phases as well as the local bonding environments in metastable and stable phases. While both mass spectrometry and spectroscopy are unable to differentiate

between localized regions of differing chemical interactions, they provide an averaged overview of an entire system, which is powerful for monitoring nucleation and growth.

4.1.1. Mass Spectrometry (MS)

Mass spectrometry (MS) provides compositional and structural information of the initial building units in solutions that occur prenucleation. Such studies enable a molecular understanding into the mechanisms and dynamics in which metastable phases such as particles form. Electrospray ionization (ESI) is a soft ionization technique that is frequently paired with MS (i.e. ESI-MS) to minimize any damage, such as fragmentation, to the prenucleation species. In a study by Filez et al, ESI-MS was used to determine the composition of the prenucleation clusters in ZIF-67, which allowed for a greater understanding of the quantity and composition of the initial SBUs.⁵⁰ By taking measurements of sample aliquots, the mechanism in which these building units evolve to form a stable nuclei was determined to be through monomer-by-monomer addition. In a different study by Salionov et al, high resolution ESI-MS was used to monitor the growth of MIL-53(AI), which revealed how solvent byproducts play a role in the nuclei formation.¹⁴⁷ The study further uncovered the crystallization mechanism to occur through nuclei aggregation.

4.1.2 Nuclear Magnetic Resonance (NMR) Spectroscopy

Nuclear magnetic resonance (NMR) is typically used to investigate prenucleation and metastable intermediates, but can also be used to study final MOF crystals and interactions with guest species. As crystallization processes are complex, producing both liquid and solid phases, different NMR methods (i.e. solution state NMR or solid state NMR) must be used for each phase. Solution state NMR is advantageous for studying the solvent-assisted ligand exchange that occurs within the liquid phase during MOF formation. A study by Yuan et al used in situ solution-state NMR to compare the rate of linker-solvent exchange during a MOF formation in various solvents which could then be linked to the extent of defect formation in the final MOF crystals. Assistance of the state of the extent of defect formation in the final MOF crystals.

Solid-state NMR (SSNMR) can be used to study both the short-range and medium-range order. Short-range order is when atoms are ordered only over a short distance, such as during nucleation, and medium-range order is when atoms are ordered over a medium distance, such as in metastable amorphous phases.¹⁴⁹ Additionally, information on local defects and disorders on the bulk crystal can be obtained.¹⁵⁰ SSNMR is also particularly useful for providing information pertaining to the amount and position of guest molecules—such as CO₂ gas—within a framework, in addition to the chemical bonds between the MOF and guest molecule, as discussed in a review by Witherspoon et al.¹⁴⁸ Advanced NMR techniques such as high-field-SSNMR allow both liquid and solid phases to be monitored simultaneously on the molecular scale, providing insight into the nucleation and growth processes. Such methods are currently challenging for ZIFs, with SSNMR used only for characterization of the structural ordering in final ZIF structures. This is due to multiple reasons, with the three biggest being the low gamma and therefore low sensitivity, high quadrupole moment—which can lead to peak broadening and improper assignment—and low natural abundance of ⁶⁷Zn, the isotope of zinc needed for NMR spectroscopy.^{151,152} Applications of SSNMR to non-ZIF MOFs abound however; an in situ high-field SSNMR study by Jones and coworkers was successfully performed on a nickel-phosphonate MOF, as multiple NMR spectras could be monitored.¹⁵³ Through the study, NMR was used to monitor time dependent changes that occurred during MOF formation and collected kinetic information for reactions at various temperatures.

4.1.3. Infrared and Raman Spectroscopy

Infrared (IR) and Raman Spectroscopy both provide information on the molecular bindings occurring in solution and in various phases in MOF formation through measurement, by means of either scattering or absorption of the vibrational modes of the chemical bonds. Thus, influences by intrinsic or extrinsic factors can be monitored through changes in the vibration mode. IR spectroscopy relies on atoms being free to vibrate in order to detect different functional groups with known absorptions. Atoms in MOFs are locked in a crystal lattice, having different IR absorption than the free atoms. Time-resolved Fourier transform infrared spectroscopy (FTIR) has been used to measure the folding of enzymes within ZIF-8, specifically the Amide I, II, and III peaks. ¹⁵⁴ FTIR measurements can be used to determine the presence of enzymes in a p-MOF, as well as presence of CO₂, in the case of ZIF-C. ^{68,154}

Whereas IR is based on absorption of IR light, Raman Spectrometry measures vibrational modes by means of photon scattering. Raman is particularly useful for studying MOF-guest interactions in aqueous solutions, as Raman is not sensitive to water vibration which could overlap the MOF-guest vibrations. ¹⁵⁵ In situ Raman has been used to study how temperature plays a role in molecular packing and, consequently, ability to integrate guest molecules. Furthermore, a study by Kumari et al found that lower temperatures promoted greater gas adsorption in ZIF-8 due to larger windows between the methyl-imidazole rings in

the MOF building blocks.¹⁵⁶ Using a combination of both Raman and IR is most impactful, as each is sensitive to different vibrations, providing greater insight into the chemical reactions occurring in solution, and this is applicable to all MOFs. Embrechts et al used in-situ Raman and FTIR to study the nucleation and growth of MIL-53 (Al) in DMF through evolution in the vibrational bands.¹⁵⁷ Through this study, the transformation of the atomic ordering in the metastable phase to the stable crystalline nucleus could be probed.

4.2. Scattering Techniques

Scattering techniques can be performed on MOFs to obtain averaged ensemble data pertaining to the nucleation and growth kinetics of a crystallization as well as the evolution of particle size, morphology, and distribution. Data of a sample is obtained through collecting scattered radiation off a sample as a function of angle and/or time. Based on the radiation wavelength, different length scales can be obtained.

4.2.1. Light Scattering

Dynamic light scattering (DLS) and static light scattering (SLS) use light or photon radiation sources, allowing for nanometer resolution, of initial MOF species. DLS measures the scattering of light at a single angle to determine the hydrodynamic radius (R_h), which relates the diffusion of a particle in solution to the diameter of a sphere. SLS measures radiation at several angles to obtain the radius of gyration (R_g), or the radius based on a particle's center of mass. R_g allows the molecular weight of particles to be determined. Using a mathematical approximation, Saha and coworkers fit time-resolved SLS data from the growth of ZIF-71 nanoparticles to a Nucleation and Growth (NG) model. By determining the mass values of the intermediates, the NG model then provided information on how the mass of the nanoparticles evolve over time. Additionally, by using the ratio of R_g/R_h , particle morphology and shape evolution of MOF particles can be studied. 160

Light scattering techniques can further be used to measure solution turbidity by measuring the scattering intensity, enabling the rate of particle formation to be determined.²³ Zeta potential, which measures the surface charge of particles, measurements can be performed with light scattering techniques. Surface charge measurements are particularly important to understanding the electrostatics driving heterogeneous nucleations on surfaces such as biomolecules¹¹⁵ and zeolites.¹⁶¹ It is important to note that light scattering techniques are limited in that they cannot obtain accurate particle or intensity measurements in very heterogeneous and/or turbid MOF solutions. Thus controls are needed for all lights scattering methods to determine the best working concentrations of MOF samples.

4.2.2. X-ray scattering

X-ray scattering techniques use x-rays as radiation sources, enabling higher resolution than previously mentioned light scattering techniques due to the short wavelengths of X-rays compared to visible light. These methods can provide insight into the nucleation and growth mechanisms of MOFs through morphological and structural evolution studies of the amorphous and crystalline phases. X-ray diffraction is a subclass of x-ray scattering where the scattered radiation is elastic (i.e the same energy as the incident x-rays) and is limited to measuring crystalline structures. While the arrangement of amorphous species cannot be determined with XRD, the presence of the species can still be determined through broad peaks occurring in the spectra background. The rate of crystallinity can then be monitored through changes in peak intensities over time, as it gives insight into reaction pathways and observes intermediate crystalline and amorphous phases. A study by Katsensis and coworkers used insitu XRD to monitor the structural evolution of ZIF-8 while applying a mechanical stress (i.e. mechanochemical synthesis). ¹⁶² By monitoring the XRD peaks, they were able to discover new metastable phases and a deeper understanding of how structural density plays a role in polymorph transformation. Additionally, Pair distribution function analysis (PDF) of In-Situ XRD measurements is a powerful tool for measuring the interatomic distances of species present during MOF prenucleation, nucleation, and growth, and has been used to study the UiO-66 system. ⁴⁸

Small angle X-ray scattering (SAXS) and wide angle X-ray scattering (WAXS) are both types of x-ray scattering techniques which can identify crystallographic information as well as information pertaining to particle shape and size. SAXS is extremely versatile and can monitor the size and shape of initial MOF phases during nucleation and growth of MOF in the 1-100 nm range. Samples can be amorphous, semi crystalline, or crystalline, allowing for information on the initial stages of nucleation and growth that are not typically observed in XRD to be collected. In-situ SAXS is also used to track the increase in crystalline peak area over time after nucleation, offering insight into the growth rate of MOF systems and polymorphs ^{159,163}. SAXS' applications are not limited to identification of crystalline size and shape; this technique can also be used to understand the shape and function of enzymes when they are encapsulated in MOFs.¹⁶⁴ In a recent study, SAXS was used to track the microstructural changes of

hollowed MOFs to hold different enzymes and showed that the microporous region would shrink, allowing for the macropores to expand to hold the enzymes.

WAXS measurements are taken with the detector in a closer position than with SAXS, so larger diffraction angles can be monitored, which is used to look at crystalline phases. ^{163,165} WAXS has been utilized to studying the change and formation of transitory MOF structures and monitor the kinetics of MOF crystallization and growth. MOF synthesis reactions often absorb significant amounts of X-rays, limiting the amount and accuracy of data that can be collected via X-ray scattering techniques. Additionally, many laboratory X-ray sources lack the brilliance, beam coherence, and tunable wavelength ideal for studying material formation kinetics *in situ*. SAXS and WAXS also suffer from poor temporal resolution, as laboratory X-ray source measurements—especially ones with low signal-to-noise—often take minutes to hours, during which important kinetic information can become lost. While synchrotron sources can and have mitigated these issues, obtaining experiment time at these sources is difficult, and consequently, few studies of this type have been conducted. WAXS has been used mainly to monitor the growth of characteristic crystalline peaks and measure the kinetic growth. For example, it has been used to understand the formation mechanisms of a multicomponent MOFs, revealing phase transitions throughout the synthesis. ¹⁶⁶ The kinetic information gained from these experiments are crucial in the development of scaled up reactions and optimization of the synthesis.

4.2.3. Neutron Scattering

Small angle neutron scattering (SANS) has the highest resolution of the scattering techniques, allowing nanometer resolution. As it is sensitive in measuring lighter elements such as carbon and oxygen, SANS is useful in monitoring the encapsulation and structure of biomolecules in MOFs. Using SANS, the spatial arrangement of a protein was able to be determined within the pores of MOF-919, which is not possible with other scattering or microscopy techniques. ¹⁶⁷ In the study, the protein was deuterated to enhance the contrast between the protein and MOF. Additionally, SANS has been used to determine the arrangement of ions in the pores of a conductive MOF, providing insight into how to enhance the performance of the system as a capacitor. ¹⁶⁸ While SANS is a relatively new technique to studying MOFs, we foresee it having a huge impact in deciphering how guest species influence nucleation and growth mechanisms as well as further insight into how crystal structure influences the performance of guest species.

4.3. Microscopy Techniques

Microscopy methods provide images of localized regions of a sample enabling phases that occur simultaneously to be distinguished. Additionally, information on the dynamics and character of individual phases and crystals can be obtained. The resolution or viewing range of a sample is dependent on the wavelength of the beam source and the voltage at which the beam is emitted. For example, microscopes that use photons (a.k.a. visible light) rather than electrons for a beam source have lower resolution as photons have a longer de Broglie wavelength than electrons.

4.3.1. Optical Microscopy

Optical microscopes use visible light enabling samples to be viewed within the microns to millimeters range. This viewing range limits usage of this technique to characterization of final crystal size measurements and morphologies as the prenucleation and amorphous phase regimes occur within the nanometer range. Despite these limitations, optical microscopes are more accessible to researchers as their cost and maintenance is more affordable than other microscopy techniques and are more user-friendly, making them a powerful technique to study final MOF crystals. Using optical microscopy techniques, the orientation and shape of final ZIF-8, MIL-88A, and MIL-96-1 crystals could be described, providing insight into how the crystals pack onto certain substrates. In the case when large (~100µm) MOF crystals are produced, it is even possible to monitor the growth kinetics, such as in a study with MOF-5. Additionally, confocal scanning laser microscopy can be used to determine surface functionalization of guest species such as drugs 172 or biomolecules.

4.3.2. Atomic Force Microscopy

Atomic force microscopy (AFM) uses a laser probe that allows resolution 1000 times greater than that of an optical microscope. The technique produces images through direct interactions or scannings of the probe tip with the MOF surface, allowing for topological and morphological growth studies of the metastable phases and final crystals. Advancements in in-situ AFM have enabled AFM measurements to be performed in the native, solution environment of MOF crystallization.¹⁷³ Such studies have discovered, through measuring the change in surface heights, that nucleation of ZIF-8 occurs on the surface followed by spreading of a metastable phase to form a stable, crystalline phase.⁸⁷ Additionally the study provided insight into how non-

framework species, such as solvent molecules, can play a role in the stabilization and ordering of monomeric species during crystal growth. A follow up study revealed that ZIF-67, which has the same crystal structure as ZIF-8 but has a cobalt metal center rather than zinc, follows the same growth mechanism as ZIF-8.¹⁷⁴

4.3.3. Electron Microscopy

Electron microscopes utilize beams of electrons to image samples, allowing atomic scale resolution. The two main categories of electron microscopes are transmission electron microscopes (TEM) and scanning electron microscopes (SEM). These microscopes are largely differentiated based on the energy of electrons emitted. Transmission electron microscopy uses high energy electrons to pass through the sample and provide internal information such as pores and defects in the crystal structure. TEM is unique among all techniques because the lattice structure of individual phases and products can be imaged using high resolution TEM (HRTEM).¹⁷⁵ This allows amorphous phases to be distinguished from crystalline phases and provide insight into the evolution of the system.²³ Video imaging using HRTEM has also been used to elucidate molecular level information about prenucleation species in MOF formation in the case of MOF 5.⁵¹ While HRTEM provides crystal structure in real-space imaging, micro electron diffraction (microED) images a sample in reciprocal space and obtains diffraction patterns, similar to that in x-ray diffraction, on selected phases of interest. ¹⁷⁶

While previously mentioned TEM methods provide 2D images of a sample, electron tomography (ET) allows the sample to be tilted at various angles within the TEM to provide a three dimensional view of the crystal structure. This method is advantageous for studying how guest molecules such as drugs and biomolecules interact with the MOF structure. For example, ET was used to understand the distribution of doxorubicin, a cancer treatment drug, within ZIF-8.6 Additionally, ET has been used to determine the mechanisms which small molecules cap onto growing crystal facets to dictate growth rate and final crystal morphology. 136

MOFs can be a challenge to image with TEM, especially at high resolution, as the high electron energy can damage the crystal structure. ^{175,177} To combat the beam sensitivity of MOFs, cryogenic TEM (cryo-TEM) has been used to improve beam stability of the specimen. In this technique, aliquots of samples are brought to cryogenic temperatures, providing a snapshot of the reaction at certain time points. ¹⁷⁵ To provide further information into the kinetics and dynamics of a crystallization in real-time, liquid phase TEM (LPTEM) can be used to visualize the growth of MOFs while in their native solution. ¹⁷⁸ Using LPTEM, Liu et al captured three key nucleation steps during the formation of MOF nanocrystals. ²² The LPTEM videos display a homogeneous solution of MOF precursors that phase separate to form a dense liquid phase. The dense liquid phase then condenses into an amorphous cluster that then undergoes crystallization. The direct observations in this study provides insight into how to better control crystallization and should be generalizable to many other MOF systems.

Scanning electron microscopy (SEM) uses lower energy electrons compared to TEM, allowing external features such as the surface morphology of the MOF crystals to be imaged, with resolution as low as 1 nm.¹⁷⁹ SEM has proved to be particularly useful for studying how the size, shape, and morphology of metastable and stable phases evolve over time. A study by Jian et al demonstrated that by modulating the rate of nucleation through precursor concentration, the shape and size of ZIF-8 crystals could be controlled.¹⁸⁰ At a set concentration, the authors monitored the morphological evolution over the course of 24 hours and observed crystal growth through Ostwald ripening as small ZIF-8 crystals disappeared overtime while larger crystals appeared. Because MOFs are not conductive materials, electrons often build up on the surface of the crystals, called "charging", producing blurry images.¹⁸¹ To reduce charging, thin coatings of conductive elements such as iridium or gold are coated onto the sample using a plasma sputter coater.¹⁸²

4.4. Computational Techniques

Computational techniques have the ability to complement each of the previously mentioned experimental techniques and can be used to predict the mechanistic pathways of each phase and phase transition. The most common computational techniques used to study MOF formation are molecular dynamic (MD) simulations. MD simulations can simulate individual atoms of the MOF precursors along with the atoms in the solution, which can provide dynamic and kinetic information on initial metalligand coordinations and how phase separation from the bulk solution occurs.²² Such information can provide valuable insight into polymorph selection. MD simulations have been commonly paired with density functional theory (DFT) calculations to extract mechanistic information on nucleation. A study by Filez and coworkers determined through pairing of MD and DFT, the initial metal-ligand complexes that occurred during ZIF-67 formation as well as the coordination environment of amorphous metastable species.⁵⁰ Balestra and coworkers also used DFT calculations in combination with MD and a calculated force field to simulate the coordination bonds occurring during nucleation and crystal decomposition of ZIF-8.¹⁸³ This simulation found that ZIF-8 first forms

small clusters, then dissolves into an amorphous precursor from which larger clusters form, which has been verified with TEM studies.²³

Monte Carlo simulations can also be used to investigate individual atoms of the MOF precursors and solution, similar to MD, but varies in its simulation approach. A study by Wells and coworkers developed an algorithm using Monte Carlo simulations and discovered different phases with varying topologies could be formed as a result of manipulating the metal-ligand ratio.¹⁸⁴ To understand the mechanisms of secondary building units, large-scale MD simulations have been performed using graph theory models to understand the formation mechanisms in various reaction conditions. Kollias and coworkers have simulated the initial nucleation stages of MIL-101(Cr) and have demonstrated how solvents and ions affect the early cluster formation, which dictates the configuration and complexity of the final MOF lattice.³³ By modeling the interactions of the building units with the free metal ion and organic linker, we can better understand MOF formation.¹⁸⁵

4.5. Summary

A wide range of tools have been deployed to study MOF nucleation and growth at all stages, from the molecular chemistry of the precursors to the final bulk crystals. Depending on the type of information required and which stage of the nucleation and growth process is of interest, different tools should be selected. Spectroscopy, mass spectrometry and computational methods are commonly deployed to understand the molecular chemistry of MOF nucleation and growth while microscopy and scattering methods are more commonly used to study the crystal growth mechanisms and kinetics. However, it is important to note that all methods can be used to study a wide range of aspects in nucleation and growth. We predict that some of these instruments, specifically electron microscopy, will become more important to the study of MOF nucleation and growth from a molecular perspective as the resolution and sensitivities increase. We also expect that mass spectrometry will play a bigger role in understanding molecular chemistry in the early stages of MOF nucleation. Importantly, a combination of instrumentation techniques should be used to elucidate high quality information about MOF nucleation and growth, and we do not predict this to change as the field advances.

5. Outlook and future directions

Compelling progress in MOF crystallization has been made in the last several years, unraveling new mechanistic insights. By combining fundamental chemistry theories with experimental and computational experiments, progress has been made in determining the structural composition of prenucleation species and the mechanisms in which these species evolve to become a bulk crystal. Progress can be largely credited to advancement of characterization methodology and instrumentation. As temporal and spatial resolution continue to improve among instrumentation, we look forward to greater insight into the nucleation and growth of crystals on both the molecular and bulk scale. Large experimental and instrumental efforts have been made to determine how reaction conditions such as solvent and temperature tailor the mechanistic pathways that govern the size, dimensionality, and structure of crystals. We anticipate innovation in expanding the current pressure and temperature limitations in instrumentation—specifically TEM and X-ray scattering—to enable systems that form under broader ranges of synthetic conditions to be better understood. Such studies would provide essential, transferable studies to industry which often use high pressure and temperature processing conditions. As we continue to develop high-throughput characterization methods, such as with the recent development of high-throughput TEM, ¹⁸⁶ the size in which data sets can be generated will advance, allowing translatable findings to a greater range of systems.

Mechanistic studies using small molecules and surfaces have revealed new mechanistic pathways in which the activation energy to nucleation can be adjusted to trap metastable and kinetic products. Additionally, countless structure-function properties have been discovered pertaining to MOF-guest species interactions, with broad implications in applications ranging from catalysis to gas storage. While MOF crystallization pathways can be exceedingly complex, especially with the introduction of a guest molecule, we anticipate large efforts in methodology and instrumentation to differentiate the multiple phases that frequently form simultaneously during crystallization. This is particularly important for enzyme incorporation as it is essential to distinguish which intermediate and final phase(s) contain the enzyme to understand the influence of the enzyme in the nucleation of each phase, to understand how it drives the growth of each phase, and to understand how (location, orientation etc.) the enzyme is incorporated into each phase. With each new discovery pertaining to how intrinsic and extrinsic factors tailor crystal formation, we encourage researchers to further explore how the synthetic volume, both in confined and large bulk volumes, alter the crystallization process. Such studies will further accelerate how we understand synthetic scaling of MOF crystals, which is key to mass production. As we are excited for the future of MOF crystallization, we anticipate relying heavily on nucleation and growth fundamentals to tap into the unexplored design space and engineer MOFs with enhanced performances.

References

- 1 H. Li, M. Eddaoudi, M. O'Keeffe and O. M. Yaghi, *Nature*, 1999, **402**, 276–279.
- 2 I. M. Hönicke, I. Senkovska, V. Bon, I. A. Baburin, N. Bönisch, S. Raschke, J. D. Evans and S. Kaskel, *Angewandte Chemie International Edition*, 2018, **57**, 13780–13783.
- 3 M. P. Suh, H. J. Park, T. K. Prasad and D.-W. Lim, Chem. Rev., 2012, 112, 782-835.
- 4 R. Aniruddha, I. Sreedhar and B. M. Reddy, Journal of CO2 Utilization, 2020, 42, 101297.
- 5 K. S. Park, Z. Ni, A. P. Côté, J. Y. Choi, R. Huang, F. J. Uribe-Romo, H. K. Chae, M. O'Keeffe and O. M. Yaghi, *Proceedings of the National Academy of Sciences*, 2006, **103**, 10186–10191.
- 6 H. Zheng, Y. Zhang, L. Liu, W. Wan, P. Guo, A. M. Nyström and X. Zou, *J. Am. Chem. Soc.*, 2016, **138**, 962–968.
- 7 K. Liang, R. Ricco, C. M. Doherty, M. J. Styles, S. Bell, N. Kirby, S. Mudie, D. Haylock, A. J. Hill, C. J. Doonan and P. Falcaro, *Nat Commun*, 2015, **6**, 7240.
- 8 F. Lyu, Y. Zhang, R. N. Zare, J. Ge and Z. Liu, *Nano Lett.*, 2014, **14**, 5761–5765.
- 9 J. Lee, O. K. Farha, J. Roberts, K. A. Scheidt, S. T. Nguyen and J. T. Hupp, *Chem. Soc. Rev.*, 2009, **38**, 1450–1459.
- 10 R. B. Getman, Y.-S. Bae, C. E. Wilmer and R. Q. Snurr, Chem. Rev., 2012, 112, 703-723.
- 11 G. Lu and J. T. Hupp, *J. Am. Chem. Soc.*, 2010, **132**, 7832–7833.
- 12 Q. Wang, Y. Sun, S. Li, P. Zhang and Q. Yao, RSC Advances, 2020, 10, 37600-37620.
- 13 S. Peng, B. Bie, Y. Sun, M. Liu, H. Cong, W. Zhou, Y. Xia, H. Tang, H. Deng and X. Zhou, *Nat Commun*, 2018, **9**, 1293.
- 14 S. M. Moosavi, A. Nandy, K. M. Jablonka, D. Ongari, J. P. Janet, P. G. Boyd, Y. Lee, B. Smit and H. J. Kulik, *Nat Commun*, 2020, **11**, 4068.
- 15 A. Zuliani, N. Khiar and C. Carrillo-Carrión, Anal Bioanal Chem, 2023, 1–19.
- 16 Y. Li and J. Yu, *Nat Rev Mater*, 2021, **6**, 1156–1174.
- 17 Y. Li, H. Cao and J. Yu, *ACS Nano*, 2018, **12**, 4096–4104.
- 18 J. Yu and R. Xu, Acc. Chem. Res., 2010, 43, 1195–1204.
- 19 A. Budiman, Z. G. Citraloka, M. Muchtaridi, S. Sriwidodo, D. L. Aulifa and A. Rusdin, *Pharmaceutics*, 2022, **14**, 2386.
- 20 F. Artusio, F. Fumagalli, A. Valsesia, G. Ceccone and R. Pisano, *ACS Appl Mater Interfaces*, 2021, **13**, 15847–15856.
- 21 M. J. Van Vleet, T. Weng, X. Li and J. R. Schmidt, Chem. Rev., 2018, 118, 3681–3721.
- 22 X. Liu, S. W. Chee, S. Raj, M. Sawczyk, P. Král and U. Mirsaidov, *PNAS*, , DOI:10.1073/pnas.2008880118.
- 23 A. F. Ogata, A. M. Rakowski, B. P. Carpenter, D. A. Fishman, J. G. Merham, P. J. Hurst and J. P. Patterson, *J. Am. Chem. Soc.*, 2020, **142**, 1433–1442.
- 24 J. J. De Yoreo, P. U. P. A. Gilbert, N. A. J. M. Sommerdijk, R. L. Penn, S. Whitelam, D. Joester, H. Zhang, J. D. Rimer, A. Navrotsky, J. F. Banfield, A. F. Wallace, F. M. Michel, F. C. Meldrum, H. Cölfen and P. M. Dove, *Science*, 2015, 349, aaa6760.
- 25 D. Kashchiev, J. Chem. Phys., 2003, 118, 1837–1851.
- 26 D. G. Vlachos and K. F. Jensen, Surface Science, 1992, 262, 359-370.
- 27 J. J. De Yoreo and P. G. Vekilov, *Reviews in Mineralogy and Geochemistry*, 2003, **54**, 57–93.
- 28 Y. Liu, Y. Yang, Y. Sun, J. Song, N. G. Rudawski, X. Chen and W. Tan, *J. Am. Chem. Soc.*, 2019, **141**, 7407–7413.
- 29 F. Millange, M. I. Medina, N. Guillou, G. Férey, K. M. Golden and R. I. Walton, *Angewandte Chemie International Edition*, 2010, **49**, 763–766.
- 30 X.-G. Wang, Q. Cheng, Y. Yu and X.-Z. Zhang, *Angewandte Chemie International Edition*, 2018, **57**, 7836–7840.

- 31 A. V. Dighe, L. Huelsenbeck, R. R. Bhawnani, P. Verma, K. H. Stone, M. R. Singh and G. Giri, *JACS Au*, 2022, **2**, 453–462.
- 32 S. L. Anderson, A. Gładysiak, P. G. Boyd, C. P. Ireland, P. Miéville, D. Tiana, B. Vlaisavljevich, P. Schouwink, W. van Beek, K. J. Gagnon, B. Smit and K. C. Stylianou, *CrystEngComm*, 2017, **19**, 3407–3413.
- 33 L. Kollias, R. Rousseau, V.-A. Glezakou and M. Salvalaglio, *J. Am. Chem. Soc.*, 2022, **144**, 11099–11109.
- 34 A. D. Katsenis, A. Puškarić, V. Štrukil, C. Mottillo, P. A. Julien, K. Užarević, M.-H. Pham, T.-O. Do, S. A. J. Kimber, P. Lazić, O. Magdysyuk, R. E. Dinnebier, I. Halasz and T. Friščić, *Nat Commun*, 2015, **6**, 6662.
- 35 S. L. Burkett and M. E. Davis, J. Phys. Chem., 1994, 98, 4647–4653.
- 36 L. B. Gower and D. J. Odom, Journal of Crystal Growth, 2000, 210, 719–734.
- 37 L. Kuhrts, S. Prévost, D. M. Chevrier, P. Pekker, O. Spaeker, M. Egglseder, J. Baumgartner, M. Pósfai and D. Faivre, *J. Am. Chem. Soc.*, 2021, **143**, 10963–10969.
- 38 R. L. Penn and J. F. Banfield, *Science*, DOI:10.1126/science.281.5379.969.
- 39 A. Aerts, C. E. A. Kirschhock and J. A. Martens, Chem. Soc. Rev., 2010, 39, 4626-4642.
- 40 M. Eddaoudi, D. B. Moler, H. Li, B. Chen, T. M. Reineke, M. O'Keeffe and O. M. Yaghi, *Acc. Chem. Res.*, 2001, **34**, 319–330.
- 41 M. J. Kalmutzki, N. Hanikel and O. M. Yaghi, Science Advances, 2018, 4, eaat9180.
- 42 G. Férey, Journal of Solid State Chemistry, 2000, 152, 37-48.
- 43 A. Schoedel, in *Metal-Organic Frameworks for Biomedical Applications*, ed. M. Mozafari, Woodhead Publishing, 2020, pp. 11–44.
- 44 S. Surblé, F. Millange, C. Serre, G. Férey and R. I. Walton, *Chem. Commun.*, 2006, 1518–1520.
- 45 J. A. Rood, W. C. Boggess, B. C. Noll and K. W. Henderson, *J. Am. Chem. Soc.*, 2007, **129**, 13675–13682.
- 46 M. W. Terban, D. Banerjee, S. Ghose, B. Medasani, A. Shukla, B. A. Legg, Y. Zhou, Z. Zhu, M. L. Sushko, J. J. D. Yoreo, J. Liu, P. K. Thallapally and S. J. L. Billinge, *Nanoscale*, 2018, 10, 4291–4300.
- 47 D. C. Cantu, B. P. McGrail and V.-A. Glezakou, Chem. Mater., 2014, 26, 6401-6409.
- 48 H. Xu, S. Sommer, N. L. N. Broge, J. Gao and B. B. Iversen, *Chemistry A European Journal*, 2019, **25**, 2051–2058.
- 49 T. Lee, Y. H. Chang and H. L. Lee, CrystEngComm, 2017, 19, 426–441.
- 50 M. Filez, C. Caratelli, M. Rivera-Torrente, F. Muniz-Miranda, M. Hoek, M. Altelaar, A. J. R. Heck, V. Van Speybroeck and B. M. Weckhuysen, *Cell Reports Physical Science*, 2021, **2**, 100680.
- 51 J. Xing, L. Schweighauser, S. Okada, K. Harano and E. Nakamura, *Nat Commun*, 2019, **10**, 3608
- 52 B. B. Skielstad, Y. Hijikata and S. Maeda, *Inorg. Chem.*, 2023, **62**, 1210–1217.
- 53 N. Stock and S. Biswas, Chem. Rev., 2012, 112, 933-969.
- 54 S. S. Park, C. H. Hendon, A. J. Fielding, A. Walsh, M. O'Keeffe and M. Dincă, *J. Am. Chem. Soc.*, 2017, **139**, 3619–3622.
- 55 A. Mittal, S. Gandhi and I. Roy, *Sci Rep*, 2022, **12**, 10331.
- 56 M. Ohring, in *Engineering Materials Science*, ed. M. Ohring, Academic Press, San Diego, 1995, pp. 431–500.
- 57 N. Yuan, T. L. Church, E. G. Brandt, N. Hedin, X. Zou and D. Bernin, *Sci Rep*, 2018, **8**, 17530.
- 58 G. Zahn, P. Zerner, J. Lippke, F. L. Kempf, S. Lilienthal, C. Schroeder, A. M. Schneider and P.- Behrens, *9198-9207*, 9198, **16**, 9198.
- 59 S. J. I. Shearan, J. Jacobsen, F. Costantino, R. D'Amato, D. Novikov, N. Stock, E. Andreoli and M. Taddei, *Chemistry A European Journal*, 2021, **27**, 6579–6592.

- 60 S. D. Bagi, A. S. Myerson and Y. Román-Leshkov, *Crystal Growth & Design*, 2021, **21**, 6529–6536.
- 61 A. J. Cruz-Cabeza and J. Bernstein, Chem. Rev., 2014, 114, 2170-2191.
- 62 E. Balog, G. Varga, Á. Kukovecz, Á. Tóth, D. Horváth, I. Lagzi and G. Schuszter, *Crystal Growth & Design*, 2022, **22**, 4268–4276.
- 63 D. Aulakh, J. R. Varghese and M. Wriedt, *Inorg. Chem.*, 2015, **54**, 8679–8684.
- 64 Q. Ke, Y. Duan, Y. Ji, D. Zhao, H. Zhang, C. Duan, L. Li and Y. Wei, *J. Chem. Eng. Data*, 2021, **66**, 3483–3492.
- 65 R. N. Widmer, G. I. Lampronti, S. Chibani, C. W. Wilson, S. Anzellini, S. Farsang, A. K. Kleppe, N. P. M. Casati, S. G. MacLeod, S. A. T. Redfern, F.-X. Coudert and T. D. Bennett, *J. Am. Chem. Soc.*, 2019, **141**, 9330–9337.
- 66 M. Tu, D. E. Kravchenko, B. Xia, V. Rubio-Giménez, N. Wauteraerts, R. Verbeke, I. F. J. Vankelecom, T. Stassin, W. Egger, M. Dickmann, H. Amenitsch and R. Ameloot, *Angewandte Chemie International Edition*, 2021, **60**, 7553–7558.
- 67 A. Deacon, L. Briquet, M. Malankowska, F. Massingberd-Mundy, S. Rudić, T. I Hyde, H. Cavaye, J. Coronas, S. Poulston and T. Johnson, *Commun Chem*, 2022, **5**, 1–10.
- 68 F. Carraro, M. de J. Velásquez-Hernández, E. Astria, W. Liang, L. Twight, C. Parise, M. Ge, Z. Huang, R. Ricco, X. Zou, L. Villanova, C. O. Kappe, C. Doonan and P. Falcaro, *Chem. Sci.*, 2020, **11**, 3397–3404.
- 69 J. Lyu, X. Gong, S.-J. Lee, K. Gnanasekaran, X. Zhang, M. C. Wasson, X. Wang, P. Bai, X. Guo, N. C. Gianneschi and O. K. Farha, *J. Am. Chem. Soc.*, 2020, **142**, 4609–4615.
- 70 Database of Zeolite Structures, http://www.iza-structure.org/databases/, (accessed January 27, 2023).
- 71 M. Eddaoudi, D. F. Sava, J. F. Eubank, K. Adil and V. Guillerm, *Chem. Soc. Rev.*, 2014, **44**, 228–249.
- 72 A. A. Bertolazzo, D. Dhabal and V. Molinero, *J. Phys. Chem. Lett.*, 2022, **13**, 977–981.
- 73 Y. Lo, C. H. Lam, C.-W. Chang, A.-C. Yang and D.-Y. Kang, *RSC Adv.*, 2016, **6**, 89148–89156.
- 74 S. Karthika, T. K. Radhakrishnan and P. Kalaichelvi, *Crystal Growth & Design*, 2016, **16**, 6663–6681.
- 75 S. Yuan, L. Feng, K. Wang, J. Pang, M. Bosch, C. Lollar, Y. Sun, J. Qin, X. Yang, P. Zhang, Q. Wang, L. Zou, Y. Zhang, L. Zhang, Y. Fang, J. Li and H.-C. Zhou, *Advanced Materials*, 2018, **30**, 1870277.
- 76 M. M. Mitrović, A. A. Žekić and M. M. Napijalo, *Journal of Crystal Growth*, 2000, **216**, 437–442.
- 77 Y. Ban, Y. Li, Y. Peng, H. Jin, W. Jiao, X. Liu and W. Yang, *Chemistry A European Journal*, 2014, **20**, 11402–11409.
- 78 Y. Zhou, Y. Ban and W. Yang, *Inorg. Chem.*, 2022, **61**, 17342–17352.
- 79 J. Sun, L. Semenchenko, W. T. Lim, M. F. Ballesteros Rivas, V. Varela-Guerrero and H.-K. Jeong, *Microporous and Mesoporous Materials*, 2018, **264**, 35–42.
- 80 H. Irving and R. J. P. Williams, *J. Chem. Soc.*, 1953, 3192–3210.
- 81 H. Irving and R. J. P. Williams, *Nature*, 1948, **162**, 746–747.
- 82 R. G. Pearson, J. Am. Chem. Soc., 1963, 85, 3533-3539.
- 83 X. Zhang, B. Wang, A. Alsalme, S. Xiang, Z. Zhang and B. Chen, *Coordination Chemistry Reviews*, 2020, **423**, 213507.
- 84 S. Ahrland, J. Chatt and N. R. Davies, Q. Rev. Chem. Soc., 1958, 12, 265–276.
- 85 D. Sharma, S. Rasaily, S. Pradhan, K. Baruah, S. Tamang and A. Pariyar, *Inorg. Chem.*, 2021, **60**, 7794–7802.
- 86 M. N. Ahamad, M. Shahid, M. Ahmad and F. Sama, ACS Omega, 2019, 4, 7738-7749.
- 87 P. Y. Moh, P. Cubillas, M. W. Anderson and M. P. Attfield, *J. Am. Chem. Soc.*, 2011, **133**, 13304–13307.

- 88 F. Ragon, H. Chevreau, T. Devic, C. Serre and P. Horcajada, *Chemistry A European Journal*, 2015, **21**, 7135–7143.
- 89 D. Banerjee, J. Finkelstein, A. Smirnov, P. M. Forster, L. A. Borkowski, S. J. Teat and J. B. Parise, *Crystal Growth & Design*, 2011, **11**, 2572–2579.
- 90 Y. J. Kim, M.-Z. Kim, S. F. Alam, A. ur Rehman, A. Devipriyanka, P. Sharma, H. R. Lee and C.-H. Cho, *Materials Chemistry and Physics*, 2021, **259**, 124021.
- 91 T. Wu, X. Bu, J. Zhang and P. Feng, Chem. Mater., 2008, 20, 7377-7382.
- 92 T. R. Cook, Y.-R. Zheng and P. J. Stang, *Chem. Rev.*, 2013, **113**, 734–777.
- 93 M. Kim, J. F. Cahill, H. Fei, K. A. Prather and S. M. Cohen, *J. Am. Chem. Soc.*, 2012, **134**, 18082–18088.
- 94 L. Kollias, D. C. Cantu, V.-A. Glezakou, R. Rousseau and M. Salvalaglio, *Advanced Theory and Simulations*, 2020, **3**, 2000092.
- 95 W. Liang, R. Ricco, N. K. Maddigan, R. P. Dickinson, H. Xu, Q. Li, C. J. Sumby, S. G. Bell, P. Falcaro and C. J. Doonan, *Chem. Mater.*, 2018, **30**, 1069–1077.
- 96 M. Malekmohammadi, S. Fatemi, M. Razavian and A. Nouralishahi, *Solid State Sciences*, 2019, **91**, 108–112.
- 97 A. Hussein, in *Essentials of Flow Assurance Solids in Oil and Gas Operations*, ed. A. Hussein, Gulf Professional Publishing, 2023, pp. 143–197.
- 98 J. W. Mullin, in *Crystallization (Fourth Edition)*, ed. J. W. Mullin, Butterworth-Heinemann, Oxford, 2001, pp. 86–134.
- 99 C.-W. Tsai and E. H. G. Langner, *Microporous and Mesoporous Materials*, 2016, **221**, 8–13.
- 100Y.-X. Sun and W.-Y. Sun, Chinese Chemical Letters, 2014, **25**, 823–828.
- 101D. J. Lewis, L. Z. Zornberg, D. J. D. Carter and R. J. Macfarlane, *Nat. Mater.*, 2020, **19**, 719–724.
- 102S. R. Venna and M. A. Carreon, Chemical Engineering Science, 2015, 124, 3–19.
- 103S. Liu, W. Xiao, C. Jin, S. Xia, W. Wang, X. Jiang, L. Li, S. Wang and C. Chen, *Applied Surface Science*, 2022, **605**, 154697.
- 104S. Kumar, Y. Pramudya, K. Müller, A. Chandresh, S. Dehm, S. Heidrich, A. Fediai, D. Parmar, D. Perera, M. Rommel, L. Heinke, W. Wenzel, C. Wöll and R. Krupke, *Advanced Materials*, 2021, **33**, 2103316.
- 105C. Altintas and S. Keskin, ACS Sustainable Chem. Eng., 2019, 7, 2739–2750.
- 106X. Zhao, X. Fang, B. Wu, L. Zheng and N. Zheng, Sci. China Chem., 2014, 57, 141–146.
- 107P. Horcajada, C. Serre, D. Grosso, C. Boissière, S. Perruchas, C. Sanchez and G. Férey, *Advanced Materials*, 2009, **21**, 1931–1935.
- 108R. Makiura, S. Motoyama, Y. Umemura, H. Yamanaka, O. Sakata and H. Kitagawa, *Nature Mater*, 2010, **9**, 565–571.
- 109E. Biemmi, C. Scherb and T. Bein, J. Am. Chem. Soc., 2007, 129, 8054-8055.
- 110T. P. Vello, M. Strauss, C. A. R. Costa, C. C. Corrêa and C. C. Bof Bufon, *Phys. Chem. Chem. Phys.*, 2020, **22**, 5839–5846.
- 1110. Shekhah, H. Wang, S. Kowarik, F. Schreiber, M. Paulus, M. Tolan, C. Sternemann, F. Evers, D. Zacher, R. A. Fischer and C. Wöll, *J. Am. Chem. Soc.*, 2007, **129**, 15118–15119.
- 112I. E. Khalil, J. Fonseca, M. R. Reithofer, T. Eder and J. M. Chin, *Coordination Chemistry Reviews*, 2023, **481**, 215043.
- 113J. Liu and C. Wöll, Chem. Soc. Rev., 2017, 46, 5730-5770.
- 114M. Lv, M. Sun, M. Wu, F. Zhang, H. Yin, Y. Sun, R. Liu, Z. Fan and J. Du, *Nano Lett.*, 2022, **22**, 9621–9629.
- 115N. K. Maddigan, A. Tarzia, D. M. Huang, C. J. Sumby, S. G. Bell, P. Falcaro and C. J. Doonan, *Chem. Sci.*, 2018, **9**, 4217–4223.
- 116O. Shekhah, L. Fu, R. Sougrat, Y. Belmabkhout, A. J. Cairns, E. P. Giannelis and M. Eddaoudi, *Chem. Commun.*, 2012, **48**, 11434–11436.
- 117F. Liu and H. Xu, *Talanta*, 2017, **162**, 261–267.

- 118M.-S. Yao, W.-X. Tang, G.-E. Wang, B. Nath and G. Xu, *Advanced Materials*, 2016, **28**, 5229–5234.
- 119O. Bim-Junior, Y. Alania, F. S. Tabatabaei, R. Frem, A. K. Bedran-Russo and P. N. Lisboa-Filho, *Langmuir*, 2022, **38**, 1600–1610.
- 120L. Tong, S. Huang, Y. Shen, S. Liu, X. Ma, F. Zhu, G. Chen and G. Ouyang, *Nat Commun*, 2022, **13**, 951.
- 121A. Huang, H. Bux, F. Steinbach and J. Caro, *Angewandte Chemie International Edition*, 2010, **49**, 4958–4961.
- 122H. T. Kwon, H.-K. Jeong, A. S. Lee, H. S. An and J. S. Lee, *J. Am. Chem. Soc.*, 2015, **137**, 12304–12311.
- 123B. P. Carpenter, A. R. Talosig, J. T. Mulvey, J. Merham and J. P. Patterson, *Chemistry of Materials*.
- 124K. Sudhakar, N. N. Reddy, T. Jayaramudu, J. Jayaramudu, A. B. Reddy, B. Manjula and E. R. Sadiku, in *Design and Applications of Nanostructured Polymer Blends and Nanocomposite Systems*, eds. S. Thomas, R. Shanks and S. Chandrasekharakurup, William Andrew Publishing, Boston, 2016, pp. 75–99.
- 125M. Kalaj, K. C. Bentz, S. Ayala, J. M. Palomba, K. S. Barcus, Y. Katayama and S. M. Cohen, *Chem. Rev.*, 2020, **120**, 8267–8302.
- 126 J. Hwang, T. Heil, M. Antonietti and B. V. K. J. Schmidt, *J. Am. Chem. Soc.*, 2018, **140**, 2947–2956.
- 127R. F. Lobo, S. I. Zones and M. E. Davis, J Incl Phenom Macrocycl Chem, 1995, 21, 47–78.
- 128R. Simancas, D. Dari, N. Velamazán, M. T. Navarro, A. Cantín, J. L. Jordá, G. Sastre, A. Corma and F. Rey, *Science*, 2010, **330**, 1219–1222.
- 129M. de J. Velásquez-Hernández, E. Astria, S. Winkler, W. Liang, H. Wiltsche, A. Poddar, R. Shukla, G. Prestwich, J. Paderi, P. Salcedo-Abraira, H. Amenitsch, P. Horcajada, C. J. Doonan and P. Falcaro, *Chemical Science*, 2020, **11**, 10835–10843.
- 130 S. Diring, S. Furukawa, Y. Takashima, T. Tsuruoka and S. Kitagawa, *Chem. Mater.*, 2010, **22**, 4531–4538.
- 131A. Schaate, P. Roy, A. Godt, J. Lippke, F. Waltz, M. Wiebcke and P. Behrens, *Chemistry A European Journal*, 2011, **17**, 6643–6651.
- 132G. D. Barmparis, Z. Lodziana, N. Lopez and I. N. Remediakis, *Beilstein J. Nanotechnol.*, 2015, **6**, 361–368.
- 133G. Wulff, Zeitschrift für Kristallographie Crystalline Materials, 1901, 34, 449–530.
- 134T.-H. Yang, Y. Shi, A. Janssen and Y. Xia, *Angewandte Chemie International Edition*, 2020, **59**, 15378–15401.
- 135 J. Cravillon, R. Nayuk, S. Springer, A. Feldhoff, K. Huber and M. Wiebcke, *Chem. Mater.*, 2011, **23**, 2130–2141.
- 136G. Zheng, Z. Chen, K. Sentosun, I. Pérez-Juste, S. Bals, L. M. Liz-Marzán, I. Pastoriza-Santos, J. Pérez-Juste and M. Hong, *Nanoscale*, 2017, **9**, 16645–16651.
- 137X. Fan, W. Wang, W. Li, J. Zhou, B. Wang, J. Zheng and X. Li, *ACS Appl. Mater. Interfaces*, 2014, **6**, 14994–14999.
- 138Y. Pan, D. Heryadi, F. Zhou, L. Zhao, G. Lestari, H. Su and Z. Lai, *CrystEngComm*, 2011, **13**, 6937–6940.
- 139F. C. Meldrum and C. O'Shaughnessy, Advanced Materials, 2020, 32, 2001068.
- 140 C. J. Stephens, S. F. Ladden, F. C. Meldrum and H. K. Christenson, *Advanced Functional Materials*, 2010, **20**, 2108–2115.
- 141M. Pang, A. J. Cairns, Y. Liu, Y. Belmabkhout, H. C. Zeng and M. Eddaoudi, *J. Am. Chem. Soc.*, 2013, **135**, 10234–10237.
- 142 J. Cui, N. Gao, X. Yin, W. Zhang, Y. Liang, L. Tian, K. Zhou, S. Wang and G. Li, *Nanoscale*, 2018, **10**, 9192–9198.
- 143J.-O. Kim, K.-I. Min, H. Noh, D.-H. Kim, S.-Y. Park and D.-P. Kim, Angewandte Chemie

- International Edition, 2016, 55, 7116-7120.
- 144N. Huang, H. Drake, J. Li, J. Pang, Y. Wang, S. Yuan, Q. Wang, P. Cai, J. Qin and H.-C. Zhou, *Angewandte Chemie International Edition*, 2018, **57**, 8916–8920.
- 145P. Silva, S. M. F. Vilela, J. P. C. Tomé and F. A. A. Paz, *Chem. Soc. Rev.*, 2015, **44**, 6774–6803.
- 146P. A. Julien, C. Mottillo and T. Friščić, Green Chem., 2017, 19, 2729–2747.
- 147D. Salionov, O. O. Semivrazhskaya, N. P. M. Casati, M. Ranocchiari, S. Bjelić, R. Verel, J. A. van Bokhoven and V. L. Sushkevich, *Nat Commun*, 2022, **13**, 3762.
- 148 V. J. Witherspoon, J. Xu and J. A. Reimer, Chem. Rev., 2018, 118, 10033-10048.
- 149NMR crystallography, edited by Robin K Harris, Roderick E. Wasylishen and Melinda J. Duer,
 - https://www.tandfonline.com/doi/epdf/10.1080/0889311X.2012.660919?needAccess=true&role=button, (accessed April 19, 2023).
- 150R. Pallach, J. Keupp, K. Terlinden, L. Frentzel-Beyme, M. Kloß, A. Machalica, J. Kotschy, S. K. Vasa, P. A. Chater, C. Sternemann, M. T. Wharmby, R. Linser, R. Schmid and S. Henke, *Nat Commun*, 2021, **12**, 4097.
- 151R. S. K. Madsen, A. Qiao, J. Sen, I. Hung, K. Chen, Z. Gan, S. Sen and Y. Yue, *Science*, 2020, **367**, 1473–1476.
- 152F. H. Larsen, J. Skibsted, H. J. Jakobsen and N. Chr. Nielsen, *J. Am. Chem. Soc.*, 2000, **122**, 7080–7086.
- 153C. L. Jones, C. E. Hughes, H. H.-M. Yeung, A. Paul, K. D. M. Harris and T. L. Easun, *Chem. Sci.*, 2021, **12**, 1486–1494.
- 154W. Liang, H. Xu, F. Carraro, N. K. Maddigan, Q. Li, S. G. Bell, D. M. Huang, A. Tarzia, M. B. Solomon, H. Amenitsch, L. Vaccari, C. J. Sumby, P. Falcaro and C. J. Doonan, *J. Am. Chem. Soc.*, 2019, **141**, 2348–2355.
- 155K. I. Hadjiivanov, D. A. Panayotov, M. Y. Mihaylov, E. Z. Ivanova, K. K. Chakarova, S. M. Andonova and N. L. Drenchev, *Chem. Rev.*, 2021, **121**, 1286–1424.
- 156G. Kumari, K. Jayaramulu, T. K. Maji and C. Narayana, *J. Phys. Chem. A*, 2013, **117**, 11006–11012.
- 157H. Embrechts, M. Kriesten, K. Hoffmann, W. Peukert, M. Hartmann and M. Distaso, *J. Phys. Chem. C*, 2018, **122**, 12267–12278.
- 158J. Cravillon, S. Münzer, S.-J. Lohmeier, A. Feldhoff, K. Huber and M. Wiebcke, *Chem. Mater.*, 2009, **21**, 1410–1412.
- 159S. Saha, M. Wiebcke and K. Huber, Crystal Growth & Design, 2018, 18, 4653–4661.
- 160 S. Saha, S. Springer, M. E. Schweinefuß, D. Pontoni, M. Wiebcke and K. Huber, *Crystal Growth & Design*, 2016, **16**, 2002–2010.
- 161P. Netzsch, R. Ettlinger and R. E. Morris, APL Materials, 2023, 11, 031115.
- 162A. D. Katsenis, A. Puškarić, V. Štrukil, C. Mottillo, P. A. Julien, K. Užarević, M.-H. Pham, T.-O. Do, S. A. J. Kimber, P. Lazić, O. Magdysyuk, R. E. Dinnebier, I. Halasz and T. Friščić, *Nat Commun*, 2015, **6**, 6662.
- 163 J. Cravillon, C. A. Schröder, R. Nayuk, J. Gummel, K. Huber and M. Wiebcke, *Angewandte Chemie International Edition*, 2011, **50**, 8067–8071.
- 164S.-Y. Chen, W.-S. Lo, Y.-D. Huang, X. Si, F.-S. Liao, S.-W. Lin, B. P. Williams, T.-Q. Sun, H.-W. Lin, Y. An, T. Sun, Y. Ma, H.-C. Yang, L.-Y. Chou, F.-K. Shieh and C.-K. Tsung, *Nano Lett.*, 2020, **20**, 6630–6635.
- 165E. Stavitski, M. Goesten, J. Juan-Alcañiz, A. Martinez-Joaristi, P. Serra-Crespo, A. V. Petukhov, J. Gascon and F. Kapteijn, *Angewandte Chemie International Edition*, 2011, **50**, 9624–9628.
- 166B. He, L. K. Macreadie, J. Gardiner, S. G. Telfer and M. R. Hill, *ACS Appl Mater Interfaces*, 2021, **13**, 54284–54293.
- 167X. Wang, L. He, J. Sumner, S. Qian, Q. Zhang, H. O'Neill, Y. Mao, C. Chen, A. M. Al-Enizi,

- A. Nafady and S. Ma, Nat Commun, 2023, 14, 973.
- 168L. He, L. Yang, M. Dincă, R. Zhang and J. Li, *Angewandte Chemie International Edition*, 2020, **59**, 9773–9779.
- 169 D. Lyu, W. Xu, J. E. L. Payong, T. Zhang and Y. Wang, *Nat Commun*, 2022, **13**, 3980.
- 170M. T. Conato and A. J. Jacobson, *Microporous and Mesoporous Materials*, 2013, **175**, 107–115.
- 171W. Schrimpf, J. Jiang, Z. Ji, P. Hirschle, D. C. Lamb, O. M. Yaghi and S. Wuttke, *Nat Commun*, 2018, **9**, 1647.
- 172J. Zhuang, C.-H. Kuo, L.-Y. Chou, D.-Y. Liu, E. Weerapana and C.-K. Tsung, *ACS Nano*, 2014, **8**, 2812–2819.
- 173L. D. B. Mandemaker, M. Filez, G. Delen, H. Tan, X. Zhang, D. Lohse and B. M. Weckhuysen, *J Phys Chem Lett*, 2018, **9**, 1838–1844.
- 174R. Wagia, I. Strashnov, M. W. Anderson and M. P. Attfield, *Crystal Growth & Design*, 2018, **18**, 695–700.
- 175L. Liu, D. Zhang, Y. Zhu and Y. Han, Commun Chem, 2020, **3**, 1–14.
- 176D. Shi, B. L. Nannenga, M. G. ladanza and T. Gonen, *eLife*, 2013, **2**, e01345.
- 177C. Wiktor, M. Meledina, S. Turner, O. I. Lebedev and R. A. Fischer, *J. Mater. Chem. A*, 2017, **5**, 14969–14989.
- 178 J. P. Patterson, P. Abellan, M. S. Denny, C. Park, N. D. Browning, S. M. Cohen, J. E. Evans and N. C. Gianneschi, *J. Am. Chem. Soc.*, 2015, **137**, 7322–7328.
- 179A. E. Vladár, M. T. Postek and B. Ming, Microscopy Today, 2009, 17, 6–13.
- 180M. Jian, B. Liu, R. Liu, J. Qu, H. Wang and X. Zhang, RSC Adv., 2015, 5, 48433–48441.
- 181A. Rizvi, J. T. Mulvey, B. P. Carpenter, R. Talosig and J. P. Patterson, *Chem. Rev.*, 2021, **121**, 14232–14280.
- 182J. I. Goldstein, D. E. Newbury, P. Echlin, D. C. Joy, A. D. Romig, C. E. Lyman, C. Fiori and E. Lifshin, in *Scanning Electron Microscopy and X-Ray Microanalysis*, Springer US, Boston, MA, 1992, pp. 671–740.
- 183S. R. G. Balestra and R. Semino, J. Chem. Phys., 2022, 157, 184502.
- 184S. A. Wells, N. F. Cessford, N. A. Seaton and T. Düren, RSC Adv., 2019, 9, 14382–14390.
- 185L. Kollias, D. C. Cantu, M. A. Tubbs, R. Rousseau, V.-A. Glezakou and M. Salvalaglio, *J. Am. Chem. Soc.*, 2019, **141**, 6073–6081.
- 186X. Gong, K. Gnanasekaran, K. Ma, C. J. Forman, X. Wang, S. Su, O. K. Farha and N. C. Gianneschi, *J. Am. Chem. Soc.*, 2022, **144**, 6674–6680.